Measurements of Aerosol Optical Depth over the North Atlantic Ocean: Correlations with Surface Aerosol Concentrations

Ellsworth J. Welton [1], Kenneth J. Voss [1], Dennis L. Savoie [2], and Joseph M. Prospero [2]

1. University of Miami, Physics Department, Miami, Fl
2. University of Miami, Rosenstiel School of Marine Atmospheric Science, Miami, Fl

Abstract:

The optical properties of atmospheric aerosols are an important element of the global radiation balance and in applications such as remote sensing. One of the most important optical properties is the aerosol optical depth (AOD) and it's associated wavelength dependence, characterized by the Angstrom exponent α. Long term measurements of these aerosol features taken at various locations are necessary to track seasonal patterns of aerosol optical behavior and to determine characteristic differences in the optical properties of different sites. An AOD measurement program was begun in August of 1993 to determine the optical properties of aerosols over existing Atmosphere/Ocean Chemistry Experiment (AEROCE) sites in Miami (Florida), Bermuda, and Barbados. A description of the optical program, instrumentation and calibration procedures, and the methodology employed to determine the AOD and α are presented. Analysis of the AOD and Angstrom exponents in terms of seasonal variations and correlations with surface concentration measurements is also presented. Seasonal variations in the optical properties of the aerosols were found to be due to seasonal changes in the types and concentrations of specific aerosol species. The correlational analysis has shown that under certain circumstances aerosol species may be identified over the ocean based on analysis of the AOD and Angstrom exponent.

1. Introduction

There is relatively little information on the climatology of atmospheric aerosols, particularly over the ocean. However, the radiative effects of marine aerosols directly alter terrestrial optical properties, such as the planetary albedo, and may play an important role, directly and indirectly, in the global climate [*Charlson,* 1992]. In addition to this climatic impact, marine aerosols also affect our ability to extract surface information from satellites, in particular for ocean color remote sensing [*Gordon,* 1997]. Knowledge of the aerosol optical properties are necessary to correct for these effects in both Global Circulation Models and in satellite correction algorithms.

The most commonly measured aerosol optical property is the aerosol optical depth (AOD), which determines how the aerosol attenuates the direct solar beam. The total optical depth, τ, at a particular wavelength is defined by

$$\tau = \frac{1}{m(\theta)} \ln\left(\frac{E_o}{E}\right) \qquad (1)$$

where $m(\theta)$ is the airmass at zenith angle θ, E_o is the extra-terrestrial solar irradiance (solar constant), and E is the direct, unscattered and unabsorbed solar irradiance at the surface. For wavelengths that lie outside the usual atmospheric gas absorption bands, the total optical depth may also be written as the sum

$$\tau = \tau_R + \tau_O + \tau_A \qquad (2)$$

where τ_R is the Rayleigh optical depth due to molecular scattering, τ_O is the Chappius band ozone optical depth, and τ_A is the aerosol optical depth. The basic experimental method of acquiring the AOD from the total optical depth has been outlined in several papers, most notably Shaw [1979] and King et al. [1980].

Measurements of aerosol optical depths [*King et. al.,* 1978; *Hoppel et. al.,* 1990; *Kaufman,* 1993; *Dutton et. al.,* 1994; *Smirnov et. al.,* 1994, 1995], made at a variety of locations

around the globe and at wavelengths throughout the visible spectrum, have shown that the spectral dependence of the AOD often resembles a power law [*Angstrom*, 1964]:

$$\tau_A = \beta\lambda^{-\alpha} \qquad (3)$$

where τ_A is the AOD at wavelength λ, β is a scale factor, and α is the Angstrom exponent. The Angstrom exponent α may be related to the exponent of a Junge type size distribution ($dn/dr = Cr^{-(\gamma+1)}$) by

$$\gamma = \alpha + 2 \qquad (4)$$

[*Van de Hulst,* 1981]. The exponent, α, generally varies from zero to two. Lower values of α are associated with relatively more larger-sized particles than aerosol populations with higher α values.

In order to obtain long term data sets of the AOD, hand-held sunphotometers were used at existing AEROCE (Atmosphere/Ocean Chemistry Experiment) sites in Miami (Florida), Bermuda, and Barbados. AEROCE sites also measure various aerosol parameters including concentration, and mass-size distributions. The stations are located at coastal sites and, with the exception of the AOD measurements, samples are collected only during on-shore winds; thus the aerosol data should be representative of the regional oceanic aerosol. The hand-held sunphotometers were replaced with automated multi-filter rotating shadowband radiometers by the end of 1994. The shadowbands create a more complete data record as they automatically sample all day, perform a potential calibration each day (dependent on weather), and also measure diffuse irradiance. The shadowbands operated concurrently with the sunphotometers for several months during the instrument replacement process. Table 1 indicates the geographical information and time period of the sunphotometer and shadowband measurements at each site. The instrument calibration procedure, methods of data selection, aerosol optical depths, and Angstrom exponents recorded for each site are presented in this paper.

Recent measurements of aerosol optical depths have indicated a need to also analyze their other physical characteristics in order to fully understand their climatological impact [*Kaufman et. al.*, 1994; *Smirnov et. al.*, 1995]. Li et. al. [1996] have published results of short term analysis of the optical properties of aerosols in Barbados using concurrent analysis of aerosol composition and concentration levels. Also, Pueschel et. al. [1994] have performed similar analysis of stratospheric Pinatubo aerosols from aircraft observations. Finally, several other researchers [*Hoppel et. al.*, 1990; *Smirnov et. al.*, 1995] have used synoptic air mass analysis to describe aerosol radiative measurements. However, there have been no long term studies of the relationship between aerosol optical depth measurements and the concentration of specific aerosol species.

The radiative properties of aerosols are a function of two main factors: the composition of the aerosols, and the aerosol production mechanisms. The magnitude of the AOD is proportional to the concentrations of the aerosols (the scale factor, β). The Angstrom exponent is dependent on the production mechanisms of each aerosol species. Aerosol concentrations are available for each AEROCE site. Correlations between concurrent measurements of the AOD and aerosol concentrations and resulting seasonal dependencies are also presented in this paper. The goal of the correlational analysis was to determine if it is possible to distinguish between different aerosol species based only on analysis of the AOD and Angstrom exponent (two parameters readily available from satellite remote sensing programs).

2. Instrumentation Description

Two different instruments were deployed at each AEROCE site: sunphotometers, and Multi-filter Rotating Shadowband Radiometers (shadowbands). The instruments were used to determine the total optical depth from measurements of the direct sunlight using Eq. (1). The AOD was calculated from the total optical depth using Eq. (2). Sunphotometers were first installed at each AEROCE site in the Fall of 1993. The sunphotometers were replaced with shadowbands by the end of 1994.

2.1 Sunphotometers

The sunphotometers [*d'Almeida et al.*, 1983] were manufactured by NOLL GMBH in Germany, and were provided by John DeLuisi at CMDL-NOAA. The sunphotometers used in this study had nine interference filters, with passbands approximately 5 nm wide, centered at the wavelengths shown in Table 2. Identical filters, selected from the same lot, were used in each sunphotometer and were selected to avoid water vapor absorption bands. The sunphotometers are operated manually by pointing the instrument at the sun. The operator then moves the instrument in small circles around the central direction of the sun. The instrument retains the highest signal measured and displays this reading, which is the direct sun signal that is used to determine the optical depth. The operator performs direct sun measurements for each filter in the sunphotometer. The signal, filter number, instrument temperature, and the time in GMT (either from an accurate watch or the instrument display) are recorded and then the process is repeated for the remaining filters.

2.2 Shadowbands

The shadowbands were designed by Lee Harrison and Joe Michalsky at SUNY/Albany and were manufactured by Battelle Labs in Richland, WA. A complete description of the shadowbands may be found in Harrison et al. [1994]. Shadowbands measure total downwelling irradiance and the diffuse irradiance by shadowing the irradiance collector. The direct irradiance, determined by subtracting the diffuse irradiance from the total irradiance, is then used to determine the spectral optical depth. The shadowbands are autonomous instruments designed to operate remotely in the field and are controlled via a phone line modem link. The shadowband consists of two main components: a control unit, and detector platform. The detector platform holds the band motor and detector housing. The detector housing holds the irradiance collector and seven photodiode detectors. Six of the seven photodiode detectors have spectral interference filters encapsulated with the detector. The filter wavelengths, with passbands 10 nm wide, are given in Table 2. Filter 1, a broadband filter, and filter 7, a water vapor band filter, were not used in this study. Filters 2 to 6

were chosen to avoid water vapor absorption bands. The filters are positioned so that they view the back of the irradiance collector. Measurements are performed with the 7 filters simultaneously.

2.3 Aerosol Concentration Measurements

Ground-based aerosol concentration samples are collected by drawing air through 20x25 cm Whatman 41 (W41) filters at a flow rate of about 1.1 m^3 min^{-1}, yielding average sampled volumes of about 1500 m^3. W41 filters have collection efficiencies greater than 90% for nss sulfate and ammonium, 95% for nitrate and sea-salt [*Savoie,* 1984], and 95% for mineral aerosol [*Arimoto et al.*, 1996]. At all sites, the aerosol sampler is linked to a wind sensor which controls the operation of the sampler so that it is activated only when the wind blows from the open ocean sector at a speed greater than 1 m/s. Filters are returned to Miami were they are extracted with deionized water and the extracts analyzed for major soluble inorganic ions: Na^+ by flame atomic absorption and Cl^-, NO_3^-, $SO_4^=$ by suppressed ion chromatography [*Savoie et al.,* 1989] and NH_4^+ by automated colorimetry. Non sea-salt sulfate (nss $SO_4^=$) is calculated: [total $SO_4^=$] - [Na^+ * 0.2517], where 0.2517 is the $SO_4^=/Na^+$ mass ratio in bulk sea water. The extracted filters were then placed in a muffle furnace for about 14 hours at 500°C; the residue weight (less filter blank) is assumed to be mineral dust ash.

3. Sunphotometer and Shadowband Calibrations

The instruments described in Section 2 must be calibrated before beginning analysis of the data taken with them. For the purposes of this study, the term calibration refers to all procedures that must be performed upon the instrument in order to determine the aerosol optical depth using data acquired with the instrument. The procedures used to calibrate the sunphotometers and shadowbands are described in this section.

3.1 Sunphotometer Calibrations

The calibration of the sunphotometers involves determination of E_o (in instrument counts), also referred to as the solar constant, by using procedures based on the Langley calibration method

[*Shaw*, 1979; *King et al.*, 1980]. The sunphotometers were operated by on-site AEROCE personnel who recorded measurements at approximately 10:00 am and 3:00 PM local time respectively. Therefore, normal instrument operations do not acquire enough data to perform Langley calibrations. Specific Langley measurements had to be performed with each instrument from the Miami, Bermuda, and Barbados AEROCE sites. An additional sunphotometer was used for calibration processes during and after the measurement period.

Initially the Langley method was used to perform the calibrations, for each sunphotometer, in Miami prior to deployment into the field. The instruments were then sent into the field, and operations began as indicated in Table 1. With the exception of poor weather days, the measurements continued uninterrupted for the remainder of the sunphotometer program. It was difficult to perform sea-level Langley calibrations in these locations because of atmospheric variability and cloudiness. Thus it was not possible to have the on-site operator perform routine Langley calibrations at the Bermuda and Barbados locations. The Miami instrument (M114) was calibrated several times during the sunphotometer program, both in Miami and in Brainard Lake, Colorado. An additional sunphotometer (M119), not tied to any location, was extensively calibrated during an oceanographic cruise, off of Hawaii, in October and November of 1994. Post-calibrations for the Bermuda and Barbados instruments were performed in Miami at the end of the sunphotometer program (through a method described below).

A calibration history for each instrument was compiled in order to account for time shifts in the solar constants, often caused by degradation of the filters. The calibration record for an instrument consists of a plot of the date versus E_o for the length of the entire data set. For the period when the instruments were deployed, calibration values were obtained by an interpolation between the initial calibrations and the post-calibrations. Prior experience with the degradation of sunphotometer interference filters led to the use of an exponential function for the interpolation of the calibration constants. An error correction procedure was then employed for both instruments to modify the conventional Langley calibrations.

It was difficult to perform full Langley calibrations on the instruments at the end of the sunphotometer program due to poor weather. The Miami instrument was calibrated several times during the initial startup, and throughout the program, and was considered to be the best calibrated of the sunphotometers. The M119 sunphotometer was well calibrated, using the Langley procedure, during October and November 1994 and was used to calibrate the Miami instrument at the end of the sunphotometer program through a cross-calibration procedure. A cross-calibration assumes that two identical sunphotometers are present; one is fully calibrated and is referred to as the reference instrument, while the other is uncalibrated and referred to as the target instrument. Simultaneous direct beam measurements are made with each sunphotometer at the same location. The resulting equations for each instrument are

$$E_r = E_{ro}\exp[-m_r(\theta)\tau] \quad , \tag{5}$$

$$E_t = E_{to}\exp[-m_t(\theta)\tau] \quad , \tag{6}$$

where the *r* subscript denotes the reference instrument and the *t* subscript denotes the target instrument. As E_{ro} is known, the τ is calculated using the calibrated reference instrument. Once the TOD is determined, E_{to}, can be written as

$$E_{to} = E_{ro}\frac{E_t}{E_r}\exp\left[-\tau\left(m_t(\theta) - m_r(\theta)\right)\right] \tag{7}$$

for each wavelength of the uncalibrated target sunphotometer. This cross-calibration procedure was useful because the weather need only be stable and cloud-free for a small window of time. Ideally, the target and reference measurements should be made at exactly the same time so the two airmass values are equal, the exponential term is zero, and τ need not be determined. However, exactly simultaneous measurements are often not possible, therefore, the reference and target airmass values should be as close as possible to avoid errors in calculating E_{to}.

The Miami instrument, (M114), was cross-calibrated against M119 at the end of the program and the cross-calibrations were added to the calibration history for M114. Sunphotometer

M114 was then used as a reference instrument during cross-calibrations for the Bermuda and Barbados sunphotometers. These cross-calibrations were then added to the calibration history for Bermuda and Barbados. The calibration histories for each sunphotometer at the three locations are given in Figures 1a, 1b, and 1c. The solid line is the exponential fit to the calibrations given above.

An error correction procedure was developed to fine tune these solar constants. This procedure assumes that there is some error, χ, present in the solar constant for each wavelength, and that the aerosols above the sites, on average, obey the Angstrom spectral dependence. Redefining the solar constant in terms of this error and the true solar constant yields

$$E_o = \chi E_o' \quad , \tag{7}$$

where E_o is the previously derived solar constant, χ is the error factor, and E_o' is the true solar constant. The measured τ is given by

$$\tau = \frac{1}{m(\theta)} \ln\left(\frac{E_o}{E}\right) = \frac{1}{m(\theta)} \ln\left(\frac{E_o'}{E}\right) + \frac{\ln(\chi)}{m(\theta)} \quad , \tag{8}$$

using Eq. (7). The first term on the RHS of Eq. (8) is the true TOD (τ') as follows from using Eq. (1) and Eq. (7), therefore, the following equation is calculated

$$\ln(\chi) = [\tau - \tau']m(\theta) \quad , \tag{9}$$

relating the error factor, χ, to the difference in measured and true total optical depths. τ_R and τ_O are subtracted from both the measured and true total optical depths since they are known. The resulting equation

$$\ln(\chi) = [\tau_A - \tau_A']m(\theta) \quad , \tag{10}$$

relates the error factor, χ, to the difference in measured and true aerosol optical depths.

In the calibration process, a sunphotometer reading consisted of recording, E, for each of the nine wavelengths. The AOD was then fit to Eq. (3), determining β and α, and this equation was then used to generate τ'_A, producing the final relation

$$\ln(\chi) = [\tau_A - \beta\lambda^{-\alpha}]m(\theta) \quad . \qquad (11)$$

Therefore, $\ln(\chi)$, is the difference between the measured AOD and the Angstrom fitted AOD for a given wavelength, times the airmass. This factor determines the variation from the Angstrom power law for that particular measurement.

The AOD, for each location's entire data set, was first calculated using the original solar constants from the calibration histories, and Rayleigh optical depths determined using Hansen and Travis [1974] and ozone models provided by Klenk et al. [1983]. For each day, the deviation of the AOD from the Angstrom power law was determined using Eq. (11) and the error factor, χ, was calculated. The time history of χ was fit by another exponential function, yielding an equation for χ for each instrument. This equation was used to correct the solar constants according to Eq. (7). The error-corrected solar constant histories are plotted in Figures 1a, 1b, and 1c as the dotted lines.

Channels one (380.2 nm) and nine (1025.9 nm) were not processed, and were not used in this study. The 380.2 nm filter degraded rapidly in all instruments and was considered unusable. Channel nine deviated significantly from the Angstrom power law, perhaps due to the weak water vapor absorption band around 1000 nm [*Shaw*, 1979] which was not considered in our analysis, or the effects of sea spray [*Villevalde et al.*, 1994]. These error-corrected calibration values are not significantly different from the original values but provide a fine-tuning adjustment.

3.2 Shadowband Calibrations

The shadowbands began operation in the fall of 1994. The shadowbands ran automatically, eliminating the need for an on-site operator. The Miami shadowband sampled data every minute

throughout the day. The Bermuda and Barbados shadowbands sampled every four minutes to reduce the number of data downloads per week. As the shadowbands perform measurements continually, each day offers the potential of a Langley calibration. Therefore the calibrations for the shadowbands are more complete than those for the sunphotometers since the actual daily data can be used to perform the Langley calibrations. Gaps are present in all data sets due to instrument malfunctions and the subsequent time needed to repair the problems. A gap exists in the Miami data from September 1995 to November 1995. This was caused by data communication problems and poor weather. Normal operation began again in December 1995. The Bermuda data gap, also caused by data communication problems, resulted in the loss of data from July 1995 to November 1995. The communication problems were fixed in December 1995 and shadowband operation was continued. The Barbados shadowband data set only includes data from May 1995 to August 1995 due to poor phone line connections for data transfer and unstable electrical power at the site.

All of the shadowbands collect enough data each day to perform two Langley calibrations, one in the morning and one in the afternoon, weather permitting. Therefore all that remains is to determine which of the days has weather suitable for Langley calibrations. Each shadowband's data set was analyzed using the Objective Langley Regression Algorithm (OLRA) [*Harrison and Michalsky*, 1994] in order to recover the solar constants for each instrument. The OLRA rejected a large number of the Langley calibrations for all three sites due to the variable tropical weather at each location. However, the strict criteria in the OLRA assures that the remaining Langley calibrations are accurate. Once the solar constants for each shadowband were determined using this technique, a calibration history was compiled in the same manner as for the sunphotometers. The calibration histories for each shadowband and interpolations are depicted in Figures 2a, 2b, and 2c.

There were few solar constant values recovered for the Barbados shadowband due to the small time period of the data set. Therefore, the solar constants for the Barbados shadowband were obtained by using the mean value of the solar constant for each channel instead of the interpolations described above. A linear fit to the calibration histories was performed for all of the channels except channel four (610 nm) of the Miami shadowband, and channels four and five (610 and 665

nm respectively) of the Bermuda shadowband. The filters in these channels were found to stabilize after a period of time making a single linear fit unsuitable. Instead a linear fit was performed on the first part of the calibrations, ignoring the stabilized portion, and a second linear fit was performed on the more stable portion.

These Langley calibrations were fine tuned with another procedure. This procedure assumes that there is some error, μ, present in the solar constant. Angstrom spectral dependence in the AOD was not assumed. The shadowband records more samples and with more variation in solar zenith angle than the sunphotometer, therefore, it is possible to analyze a month's worth of shadowband data to test for dependence of the AOD on solar zenith angle. We assume that the set of minimum aerosol optical depths should not depend on solar zenith angle (airmass) over the span of one month. Then the lowest optical depths on a plot of the AOD versus $1/m(\theta)$ for a given month will represent a background AOD. A linear fit to the lowest aerosol optical depths in the plot described above should have zero slope and a y intercept equal to the average background AOD for that month. A slope not equal to zero would indicate that the background AOD has some dependence on the airmass, and thus an error in the solar constant [*Ignatov,* personal communication, 1996].

Assuming that there is some error, μ, in the solar constants yields the following equation

$$E_o = \mu E'_o \quad , \tag{12}$$

where E_o is the previously derived solar constant, μ is the error factor, and E'_o is the true solar constant. Inserting Eq. (12) into Eq. (1) produces the following relation

$$\tau = \frac{\ln(\mu)}{m(\theta)} + \frac{1}{m(\theta)} \ln\left(\frac{E'_o}{E}\right) = \ln(\mu)\frac{1}{m(\theta)} + \tau' \quad , \tag{13}$$

τ' is the true optical depth as it contains the true solar constant, E_o'. The Rayleigh [*Hansen and Travis,* 1974] and ozone [*Klenk et al*., 1983] optical depths are not dependent on the calibrations so they may be subtracted from both sides of Eq. (13) to produce the equation

$$\tau_A = \ln(\mu)\frac{1}{m(\theta)} + \tau'_A \quad . \qquad (14)$$

Equation (14) may only be used when both τ_A and τ'_A represent the background (minimum) AOD. Therefore, the slope of the background AOD versus $1/m(\theta)$ plot described above is the natural logarithm of μ and the y intercept is the true background AOD (τ'_A). This procedure was used to obtain monthly values of μ for each shadowband channel. The error corrected solar constants are plotted in Figs. 2a, 2b, and 2c.

4. Aerosol Optical Depths and Concentrations

The aerosol optical depths and corresponding Angstrom exponents were calculated for the AEROCE sites in Miami, Bermuda, and Barbados using both the sunphotometer and shadowband data. The uncorrected and the error corrected calibrations described in sections 3.1 and 3.2, were applied to the data sets separately in order to gauge the usefulness of each error correction method. Data screening procedures were then used to remove optical data affected by atmospheric phenomena other than aerosols, such as clouds. Both data screening procedures were similar, but due to the nature of the instruments, a different screening procedure was employed for each instrument. The screening procedures and comparisons between the uncorrected and error corrected results are described below. The tolerance criteria in each of the data screening processes were a compromise between eliminating questionable data and retaining enough of the data set to analyze. Finally, the resulting AOD and Angstrom exponents were correlated with surface measurements of the specific aerosol species concentrations for each site.

4.1 Sunphotometer Data Screening Procedure

The aerosol optical depths and Angstrom exponents were calculated for channels two through eight, for the respective data sets, due to the calibration problems with channels one and nine. The sunphotometer data screen contained three levels. Level One determined the deviation of

the measured τ_A from the power-law-fitted τ'_A for a given measurement, similar to the error factor procedure above. If the magnitude of the deviation between τ_A and τ'_A was greater than 0.1, then the measured AOD at that wavelength was rejected. This was done to screen out AOD measurements that varied strongly from an Angstrom power law. The aerosol optical depths that survived this level were then subjected to Level Two of the screen. It should be noted that a given measurement set consists of two series of readings, E, for each of the nine channels. This was done to ensure that atmospheric properties were fairly constant during the measurement set, as the optical depth should not change appreciably during a span of five minutes (the approximate time for one measurement set). The Level Two screen examined the difference between the first and second measured aerosol optical depths. If the magnitude of the difference was greater than 0.03, then that channel was rejected. If only one of the two dual readings survived the Level One screen, then the Level Two screen was not performed. Finally, the Level Three screen determines if at least six of the seven channels (one and nine are excluded) remain, and channels two and eight are among them. If this was true then this measurement was considered usable, otherwise the entire measurement was discarded. This screening process ensures that the atmospheric aerosol properties are fairly constant during the measurement, that the AOD roughly resembles an Angstrom power law formula, and that there are enough remaining aerosol optical depths to accurately perform a fit to the Angstrom power law (for the wavelength range, 412.2 nm to 861.8 nm only). The AOD was then calculated from the surviving measurements and used to generate the Angstrom parameters. The remaining AOD values and the Angstrom exponent were then stored for that sample.

4.2 Shadowband Data Screening Procedure

The shadowbands record data continuously throughout the day, as opposed to the sunphotometer's singular morning and afternoon measurements. Therefore, a different screening method to eliminate bad data was developed. This method was based on the Sliding Window

Optical Depth Procedure (SWODP) [*Schlemmer*, personal communication, 1996] developed at the Atmospheric Sciences Research Center at the State University of New York, Albany.

The University of Miami SWODP (MSWODP) used the aerosol optical depths for each sampled measurement by the shadowband. The MSWODP then analyzed one day at a time, starting with the first measurement sample. The term, "sliding window," originated because the MSWODP analyzed a twenty minute "window" of data to determine if the window contained usable data (free from cloud contamination). Two screening levels were then applied to the resulting AOD window by the MSWODP. Level One performed a linear least squares fit to the AOD (versus time), and then calculated the individual AOD deviations from the fit. If all of the aerosol optical depths were within 0.01 of the linear fit, then the MSWODP proceeded to the Level Two screen for that window. If Level One failed, then the MSWODP slid the window ahead one sample measurement and began the screening process anew. If Level One was successful then the MSWODP applied Level Two, which determined the mean AOD for that window. If the mean AOD was less then 1.0 then the MSWODP recorded the mean AOD and corresponding Angstrom exponent for that window. If the mean AOD was greater than or equal to 1.0 then the entire window was rejected, and no data were recorded for that window of time (possible cloud presence). Regardless of the outcome of Level Two, the MSWODP then slid the window ahead by twenty minutes to the corresponding sample measurement, and the process was started over again. The MSWODP yields twenty minute averages of the AOD, and the corresponding Angstrom parameters for each day in the data set. This analysis procedure results in aerosol optical depths that do not vary erratically, that were reasonable magnitudes for atmospheric aerosols, and excluded clouds. The remaining AOD values and the Angstrom exponent were then stored for the time of day falling at the center of the twenty minute window.

4.3 Comparison of Uncorrected and Error Corrected Results

The spectral variation of the aerosol optical depths for each sunphotometer and shadowband were analyzed to compare differences between the uncorrected and error corrected (solar constant) results. The AOD values were plotted versus the wavelengths and the Angstrom fit

was applied to the data. The comparison focused on examining any changes to the Angstrom fit caused by the application of the error correction procedure.

The uncorrected sunphotometer results are not much different from the error corrected results, indicating that the data were not changed significantly by the error correction procedure. However, a small improvement to the Angstrom power law fit was obtained using the error corrected sunphotometer results. The average chi-squared data fitting parameter for each data set indicated a better power law fit. The Miami chi-squared data fitting parameter was 0.086 for the uncorrected results and 0.034 for the error-corrected results. The Bermuda uncorrected and error-corrected chi-squared parameters were 0.065 and 0.012 respectively. Finally, the Barbados uncorrected and error-corrected chi-squared parameters were 0.744 and 0.058. The sunphotometer error correction procedure assumes that the true AOD follows the Angstrom power law. Furthermore, the sunphotometer data screen explicitly screened out days (for both uncorrected and error corrected results) that did not accurately fit the Angstrom power law. For these two reasons, an improvement in the fits to the Angstrom power law between uncorrected and error corrected results was expected.

There were significant differences between the uncorrected and error-corrected results for certain channels of each shadowband. However, all of the error-corrected changes also resulted in a better average Angstrom power law fit. In particular, a clear bias in channel five of the Miami shadowband was removed after using the shadowband error correction procedure. The Miami chi-squared data fitting parameter was 0.521 for the uncorrected results and 0.122 for the error corrected results. The Bermuda uncorrected and error corrected chi-squared parameters were 0.300 and 0.131 respectively. Finally, the Barbados uncorrected and error corrected chi-squared parameters were 0.071 and 0.059. The shadowband error correction procedure and the shadowband data screen did not assume any particular spectral form of the AOD. However, results obtained using the error corrected results more accurately portrayed a power law fit compared to the uncorrected results.

Level One of the sunphotometer data screen determined the deviation of the measured AOD from the Angstrom power law. Turning off Levels Two and Three of the sunphotometer data screen allowed the percentage of measurements rejected by only Level One to be determined. The Level One sunphotometer data screen rejected 3% of the Barbados measurements and 7% of the Miami and Bermuda measurements. Therefore, at all three locations, over 90% of the sunphotometer AOD measurements resembled an Angstrom power law. Also, there were significant improvements in the Angstrom power law fits using the error-corrected shadowband results compared to using the uncorrected shadowband data. This improvement indicates that the majority of shadowband AOD measurements also resembled an Angstrom power law, particularly since no spectral dependence of the AOD was assumed but the error corrected data more accurately fit the Angstrom power law. As a result of this analysis, the majority of the aerosol optical depths measured over Miami, Bermuda, and Barbados were able to be fit to an Angstrom power law in the wavelength range 400 nm to 860 nm.

4.4 AOD and Concentration Correlation Procedure

The optical data were analyzed to determine seasonal patterns and to identify correlations with specific aerosol types and concentrations. The basic procedure was to search both the optical data and the aerosol concentration data for periods that overlapped. The aerosol sampling period was usually one day long, however in some cases the concentration measurement period was several days long. As a result, the optical data were averaged over the length of the aerosol measurement period during the correlation process. For each correlation period, the first step was to determine which aerosol types were present during the comparison period and if one appeared to be dominant. The aerosols of interest during this study were non-sea-salt sulfate (nss $SO_4^{=}$), nitrate (NO_3^{-}), sea-salt, and mineral dust.

The determination of a dominant aerosol species was based on analysis of the mass concentrations. It must be noted that sea-salt aerosols have a low mass-scattering efficiency MSE [*Li et al.*, 1996] and they are confined to the marine boundary layer. Therefore, the overall contribution of sea salt to the AOD, is generally expected to be much less than the contributions

from the other aerosol species. However, the sea-salt concentrations at each location were usually greater than the other aerosol concentrations; therefore, a direct comparison of the concentration levels alone would exaggerate the importance of sea-salt on the optical behavior. To de-emphasize the role of sea-salt aerosols, the other aerosol's concentrations were first compared to that of sea salt. First, the mean mass concentration of each aerosol at the measurement sites was calculated, the results are displayed in Table 3. If the concentration of sea salt was within 30% of it's mean value for the site in question, and the concentration of the other aerosol's was 50% less than that of the sea-salt, then sea-salt was considered to be dominant. If this initial criteria was not met, then sea-salt was excluded from the correlation and the dominant aerosol was chosen from the remaining aerosol species by assigning dominance to the aerosol with a concentration at least 50% greater than that of the other aerosols. If both the sea-salt comparison and the remaining aerosols comparison failed to determine a dominant aerosol, then that period was discarded. If a particular aerosol was found to be dominant then the optical effects recorded during that period were attributed to this aerosol species.

Analysis of the correlated data sets was undertaken to study how the AOD and Angstrom exponents vary during periods of dominance by different aerosol species. Relative increases or decreases in dominant aerosol concentrations from one period to the next should correlate with corresponding increases or decreases in the AOD. Also, long term measurements of the near-surface concentrations of aerosols have shown that individual aerosol types often have characteristic size distributions [*Savoie et al.*, 1982; *Kaufman et al.*, 1994]. Non-sea-salt sulfate particles are primarily found in the submicron range with mass-median diameters generally below 0.5 microns. Dust particles over the ocean (that is, 1000 km or more from the sources) typically have a mass median diameter of several microns or larger, although there is a substantial sub-micron component [*Li et al.*, 1996]. Sea-salt aerosols also are predominantly supramicron, with a mass median diameter in 4-6 microns. Therefore, periods of non-sea-salt sulfate dominance should contain particles that are primarily submicron and thus should yield a higher Angstrom exponent relative to a period when sea-salt or dust is the dominant aerosol; as in the latter case the particles

would primarily be at least several microns in size. It should be noted that another primary anthropogenic aerosol is nitrate. While nitrate aerosols are derived from gaseous precursors, as are non-sea-salt sulfates, in the marine environment the nitrate size distribution follows the surface area of sea-salt aerosols [*Savoie et al.*, 1982] due to a tendency of the nitrate precursors to adsorb into existing sea-salt particles. Also, nitrate concentrations were relatively low at all sites except Miami (Table 3). The majority of Miami periods of high nitrate concentrations correlated with moderate to high sea-salt concentrations. Therefore, nitrate aerosols were not analyzed in the correlation process.

4.5 AOD and Concentration Correlation Results

The monthly averaged AOD at 500 nm, the Angstrom scale factor β, and the Angstrom Exponent α, along with their respective standard deviations (σ_i) are presented for Miami, Bermuda, and Barbados in Tables 4a, 4b, and 4c. The AOD data from Table 4 are displayed for Miami, Bermuda, and Barbados in Figures 3a, 4a, and 5a, respectively. This data is the result of combining the data sets from the sunphotometers and the shadowbands for each site.

Figures 3a, 4a, and 5a show characteristic increases in the AOD during the summer months with minimum AOD values during the winter months. The relative changes in the AOD values for each site are the result of changes in the concentrations of particular aerosol species. Figures 3b, 4b, and 5b display the monthly mean aerosol concentrations at Miami, Bermuda, and Barbados. The high sea-salt concentrations measured at each site are evident. However, as mentioned above, the relative importance of the sea-salt to the AOD is less due to it's low MSE.

The Miami and Barbados concentration data shows the well known influence of Saharan dust transport during the summer months [*Prospero*, 1995]. The summer dust concentrations at each site are much higher than aerosol concentrations from other seasons and thus create high summertime AOD values. The decrease in dust concentrations during the winter, early spring, and late fall, results in sea-salt being the dominant aerosol most of the time. During these periods the AOD is lower due to the low MSE of sea-salt. Miami occasionally experiences non-sea-salt sulfate

dominant periods, particularly during the spring and summer, and relatively high AOD values may occur. These sulfate dominant periods often occur during the dust season and therefore analysis of the Angstrom exponent correlations (see below) is necessary to determine which aerosol is primarily responsible for the increase in AOD. Barbados was not significantly impacted by sulfate and it's AOD patterns may be understood solely on the analysis of the sea-salt and dust concentrations.

Bermuda does not show as much seasonal dependence in both AOD and aerosol concentration (except for sea-salt) as the other two sites. Dust concentrations at Bermuda were much lower than at Miami and Barbados, even during the summer months. The relative absence of much dust at Bermuda is the primary reason for the lack of strong seasonal dependence in the AOD. However, Bermuda does have a strong seasonal dependence in the sea-salt concentrations. Sea-salt dominance during the winter and fall months creates low AOD values relative to the spring months. During the spring months, non-sea-salt sulfates from North America are present. The Bermuda sulfate concentrations are lower than those seen at Miami, however, the high MSE of sulfate [*Li et al.*, 1996] creates AOD values that are high relative to the sea-salt induced AOD values at Bermuda. This results in the small seasonal AOD dependence observed for Bermuda.

The Angstrom exponents were correlated with the aerosol concentrations for each site based on the procedure described above. Table 5 displays the mean Angstrom exponent and corresponding standard deviation (σ_α) for each dominant aerosol. There were negative Angstrom exponents calculated at each site. The negative Angstrom exponents were attributed to less accurate Angstrom fitting at low AOD values since 74% of the negative Angstrom exponents correspond to AOD (at 500 nm) below 0.1 in value. The majority of the negative Angstrom exponent, higher AOD (> 0.1) data had exponents only slightly negative (- 0.1 or higher).

The non-sea-salt sulfate dominant periods at both Miami and Bermuda have mean Angstrom exponents of 1.216 and 1.012 respectively. The sea-salt and dust dominant periods at each site have mean Angstrom exponents ranging from 0.205 to 0.585 in magnitude. The high sulfate exponents relative to the sea-salt and dust exponents show the predominance of smaller

particles during the sulfate periods. Furthermore, using the standard deviations in Table 5 and combining sea-salt and dust into a "natural" aerosol type it is possible to show the difference between sulfate and natural (sea-salt and dust) aerosol exponents. Based on the analysis above, the Angstrom exponents for sulfate measurements over the ocean range from 0.863 to 1.365 while the Angstrom exponents for natural aerosols over the ocean range from 0.184 to 0.614 in value.

A goal of this research was to determine if it was possible to distinguish between different aerosol species over the ocean based only on analysis of the AOD and Angstrom exponent. As can be seen from analysis of the seasonal dependence of the AOD and aerosol concentrations and correlations with the Angstrom exponent, at the moment it is not generally possible to distinguish between specific aerosol types based solely on analysis of the AOD and Angstrom exponent. However, it is generally possible to distinguish between natural (sea-salt and dust) and sulfate aerosols over the ocean, and in specific cases of high dust concentrations it is also possible to distinguish between sea-salt and dust species over the ocean.

Figures 6a, 6b, and 6c display plots of the AOD versus the Angstrom exponent for Miami, Bermuda, and Barbados. The AOD and exponent values are daily averages of the entire data set for each site. Two characteristic patterns are evident in the figures. In both the Miami and Bermuda plots, the exponents are low at low AOD values. The exponents gradually increase in magnitude with corresponding increases in the AOD until an asymptote in exponent value is reached. The Barbados plot shows what appears to be an opposite pattern; decreasing exponents with increasing AOD values. In addition, there is a small portion of the Miami plot that shows relatively high AOD values with correspondingly low exponents, similar to the Barbados plot. The plots in Figures 6 are redisplayed in Figures 7a, 7b, and 7c after applying the correlational procedure. The data in each plot is segmented according to dominant aerosol type.

The Miami plot shows that the majority of sulfate dominant periods have high AOD values (above 0.2) and high Angstrom exponents (generally greater than 1.0). There is one low exponent sulfate period (below 0.5), but the AOD is much lower. The Miami plot also shows that the sea-salt and dust dominant periods have Angstrom exponents that are mostly below 0.5, as mentioned

above. However, it is also evident that several of the dust dominant periods also have high AOD values (approximately 0.2), while there is only one sea-salt dominant period with a high AOD.

The Bermuda plot shows a similar trend, as for Miami, for the sulfate dominant periods. The high AOD sulfate periods coincide with high Angstrom exponents (approximately 1.0). There is also one sulfate period with a low exponent (below 0.5), but this period also corresponds with a lower AOD value, as found in the Miami plot. For the purposes of this discussion, we are concerned only with strong dominant aerosol occurrences and the low sulfate AOD periods are discarded. The Bermuda sea-salt dominant periods are also similar to the Miami sea-salt periods, with lower AOD values (below 0.2) and low exponents (below 1.0). The dust dominant periods in Bermuda correspond with higher Angstrom exponents (mostly between 0.5 and 1.0) than those seen for Miami. However, the dust dominant AOD values for Bermuda are much lower on the average (mostly below 0.1) than for Miami dust dominant periods.

The Barbados plot shows very similar sea-salt dominant period behavior as that seen for Miami. Sea-salt periods have low AOD values (mean around 0.1) and low exponents (below 0.5). The dust dominant periods for Barbados show a clear pattern of decreasing Angstrom exponents with increasing AOD. As in Miami, high dust period AOD values (above 0.2) correspond to low exponents (below 0.5). The lower dust period AOD values (near 0.1) have higher Angstrom exponents (above 0.5), similar to the dust dominant trend shown for Bermuda.

General statements may be made by combining the results from each site. Figure 8 shows the AOD plotted versus the Angstrom exponent for each dominant aerosol period from all the sites. In general, strong non-sea-salt sulfate dominant periods are characterized by AOD values from 0.2 to 0.3, and Angstrom exponents from 1.0 to 1.5 in magnitude. In contrast to the sulfate periods, nearly all sea-salt dominant periods have AOD values from 0.1 to 0.2, and Angstrom exponents from 0.0 to 1.0 in magnitude. The dust dominant periods range in AOD from below 0.1 to just under 0.4 in value, and the majority of Angstrom exponents range from 0.0 to 1.0 in magnitude. The sea-salt and dust dominant periods overlap in both AOD and Angstrom exponent values for most ranges in question, and therefore are not easily distinguished. Both sea-salt and dust

dominant periods do not show the same characterization in AOD and Angstrom exponent as do sulfate dominant periods, therefore it is possible to distinguish strong non-sea-salt sulfate dominant periods from sea-salt and dust periods based only on the analysis of the AOD and Angstrom exponents.

The dust dominant periods show a characteristic trend in the AOD and Angstrom exponent. Dust dominant periods show that the Angstrom exponents are higher (from 0.5 to 1.0) for lower AOD values from 0.1 to 0.2, and that the exponents decrease in magnitude (to below 0.5) as the AOD increases to above 0.2 in value. This is equivalent to saying that on the average, the dust Angstrom exponents decrease rapidly as the dust concentration increases. This same trend does not occur for sea-salt dominant periods. Therefore, it is possible to distinguish strong dust periods from sea-salt periods because the sea-salt AOD values do not normally reach above 0.2 in magnitude. AOD values above 0.2 and corresponding Angstrom exponents below 0.5 in magnitude are a strong indication of dust dominance.

The ability to identify strong non-sea-salt sulfate dominant periods over the ocean by analysis of only the AOD and Angstrom exponent has been demonstrated. Also, the ability to distinguish strong dust dominant periods from normal sea-salt dominant periods has also been shown. The characteristic AOD and Angstrom exponent values that may be used to identify particular aerosol species over the ocean are summarized in Table 6.

5. Conclusions

The results of AOD analysis for Miami, Bermuda, and Barbados over approximately a two and a half year period of time have been presented. Together, the three sites provide good spatial coverage for the western half of the tropical North Atlantic Ocean. Also, the time period of over two years allows for good temporal coverage which is essential for proper seasonal studies. The results obtained from this work agree well with other AOD data sets taken in the North Atlantic region. For instance, the seasonality of average AOD values exhibited in the AVHRR AOD values

[*Husar et al.*, 1997] over the Caribbean and along the coast of the Southeast United States agrees with our data set.

The results obtained from correlations of the AOD with the aerosol concentrations also agree well with work done by other researchers that involved correlating AOD measurements over the ocean with air mass trajectories. Reddy et al. [1990] and Smirnov et al. [1995] have shown that air mass types from continental northern regions (such as the United States) produce high AOD (approximately 0.2) and high Angstrom exponents (> 1.0) when they move over the ocean. This result agrees well with the AOD and Angstrom exponents obtained in this work during non-sea-salt sulfate dominant periods. Also, AOD and Angstrom exponents presented by Smirnov et al. [1995] for a tropical maritime air mass (AOD ~ 0.15, α ~ 0.42) are similar to those found in this work during sea-salt dominant periods. Finally, AOD and Angstrom exponents from Reddy et al. [1990] for air masses from, or influenced by, the Saharan region (AOD ~ 0.39, α ~ 0.37; AOD ~ 0.13, α ~ 0.77), produce AOD and Angstrom exponents similar to those found in this work for dust dominant periods.

There are three primary conclusions drawn from this analysis. The first is that the spectral variation of the AOD over each site may be represented by the Angstrom power law. The second is that characteristic seasonal patterns in the AOD at each site are present and are caused primarily by seasonal changes in the types and concentrations of the aerosol species. Finally, it is possible to distinguish between different aerosol species over the ocean by analyzing the spectral variation of the AOD, particularly during strong periods of dominance by a single aerosol species.

The recent launch of ocean viewing satellite sensors such as SeaWiFS and the upcoming launch of the MODIS sensor on the EOS-AM satellite are used to determine the ocean color by measuring upwelling sunlight from the ocean. However, the sun's radiance must pass through the atmosphere before reaching the sensor. The measured radiances must be corrected for atmospheric effects in order to calculate the ocean color. An overview of atmospheric correction algorithms may be found in Gordon [1997]. The basic procedure for both single and multiple scattering algorithms

involves the determination of the correction factor ε [*Gordon,* 1997] at blue wavelengths after calculating ε in the near infared (NIR). The high degree to which the AOD measurements at each site resembled an Angstrom power law in the visible and NIR means it is possible that, for ocean color correction, the spectral variation of ε can be modeled using power-law size distributions [*Chomko and Gordon,* 1998].

The seasonal variability of the AOD must be understood to properly analyze the optical data and when using AOD for other secondary purposes, such as input to climate models and atmospheric correction algorithms. For instance, use of a typical AOD measured during a mid-summer Saharan dust passage, would not be representative of normal year-round conditions over the tropical North Atlantic Ocean. These types of problems may be avoided by proper understanding of the seasonal AOD changes. For instance, it would be best to use a typical AOD measured during mid-winter for climate studies and correction algorithms used to model normal open ocean conditions, and to use a typical AOD from mid-summer to study the pertubative effects of Saharan dust over the North Atlantic Ocean. Also, the use of correct AOD values, and hence the correct aerosol model, based on the understanding of seasonal changes in the aerosol species will improve the determination of the ocean color correction factor ε.

The measurement of spectral AOD from the ground is a relatively well known procedure, and surface based measurements of the AOD over the ocean are increasing in number as more attention is focused on understanding the climatic effects of aerosols on a global scale. Many of the sensors on upcoming satellites are capable of producing AOD values at, or near, the spectral variety of ground-based sensors. Also, satellite AOD measurements are performed only for cloud-free areas, and therefore, like surface AOD measurements, the resulting data should not be effected by cloud processing of the aerosol. Combination of both ground-based and satellite spectral AOD measurements will produce much needed global data of the AOD and Angstrom exponent, particularly over the oceans. The identification of specific aerosol species based on the analysis of

the AOD and Angstrom exponent has been shown in this study. The ability to identify aerosol species from analysis of other ground-based and satellite derived spectral AOD and the criteria in Table 6 will complement other current satellite aerosol identification programs, such as the TOMS aerosol index product [*Herman et al.*, 1997].

Future work will involve examining the transport patterns and source locations for the aerosol species investigated in this study. Also, the criteria developed in this work for identifying aerosol species based on measurements of the spectral AOD (Table 6) will be used to aid in analyzing data taken at the AERONET Cimel sunphotometer [*Holben et al.*, 1994] site in the Dry Tortugas, Florida.

Acknowledgements

The authors would like to thank the following people: Albert Chapin and Derrick Snowden for help in performing sunphotometer measurements and calibrations; Miguel Izaguirre and Tom Snowden for help in arranging site communications and logistics; Hal Maring, and Xu Li for providing useful information on aerosol measurement techniques and various aerosol properties; Joe Michalsky and Lee Harrison for providing much needed information and suggestions on performing shadowband measurements; Alexander Ignatov for providing information on the procedure used to correct the shadowband calibrations; Jim Schlemmer for providing the algorithm to the SUNY Sliding Window Optical Depth Procedure; and AEROCE site operators Anne Glasspool, Cornealius Shea, Matthew Krasowski, Megan McKay, H. B. Gooding, and Dr. F. Henriques for help in maintaining the on-site instruments. The optical measurements were funded by NASA contract #NA55-31363, and NOAA grant #NA16RCO471-01. The aerosol chemistry measurements were made under National Science Foundation grants ATM9013125 and ATM9414846.

References

d'Almeida, G.A., P. Koepke, and E.P. Shettle, *Atmospheric Aerosols: Global Climatology and Radiative Characteristics*, A. Deepak Pub., Hampton, Virginia, 1991.

Angstrom, A., The parameters of atmospheric turbidity, *Tellus*, 16, 64-75, 1964.

Arimoto, R, R.A. Duce, D.C. Savoie, J.M. Prospero, R. Talbot, J.D. Cullen, U. Tomza, N.F. Lewis, and B.J. Ray, Relationship among aerosol constituents from Asia and the North Pacific during PEM-West A, *J. Geophys. Res*., 101, 2011-2023, 1996.

Charlson, R.J., S.E. Schwartz, J.M. Hales, R.D. Cess, J.A. Coakley Jr., J.E. Hansen, and D.J. Hofmann, Climate forcing by anthropogenic aerosols, *Science*, 255, 423-430, 1992.

Chomko, R., and H. Gordon, Atmospheric correction of ocean color imagery: Use of the Junge power-law aerosol size distribution with variable refractive index to handle aerosol absorption, (In Press) *Appl. Optics*, 1998.

Dutton, E.G., P. Reddy, S. Ryan, and J. DeLuisi, Features and effects of aerosol optical depth observed at Mauna Loa, Hawaii: 1982-1992, *J. Geophys. Res.*, 99, 8295- 8306, 1994.

Gordon, H.R., Atmospheric correction of ocean color imagery in the Earth Observing System era, *J. Geophys. Res*., 102, 17081-17106, 1997.

Hansen, J.E., and L.D. Travis, Light scattering in planetary atmospheres,*Space Sci. Reviews*, 16, 527-610, 1974.

Harrison, L., J. Michalsky, and J. Berndt, The Automated multi-filter rotating shadow-band radiometer: An instrument for optical depth and radiation measurements, *Appl. Optics*, 33, 5118- 5125, 1994.

Harrison, L., and J. Michalsky, Objective algorithms for the retrieval of optical depths from ground-based measurements, *Appl. Optics*, 33, 5126-5132, 1994.

Herman, J.R., P. Bhartia, O. Torres, C. Hsu, C. Seftor, and E. Celarier, Global distribution of UV-absorbing aerosols from Nimbus-7/TOMS data, *J. Geophys. Res.*, 102, 16911-16922, 1997.

Holben, B.N., T.F. Eck, I. Slutsker, D. Tanre, J.P. Buis, A. Setzer, E. Vermote, J.A. Reagan, Y.J. Kaufman, T. Nakajima, and F. Lavenu, Multi-band automatic sun and sky scanning radiometer system for measurement of aerosols, *Proc. Sixth International Symposium Physical on Measurements and Signatures in Remote Sensing*, 75-83, 1994.

Hoppel, W.A., J. Fitzgerald, G. Frick, R. Larson, and E. Mack, Aerosol Size Distributions and Optical Properties Found in the Marine Boundary Layer Over the Atlantic Ocean,*J. Geophys. Res.*, 95, 3659-3686, 1990.

Husar, R.B., J.M. Prospero, L.L. Stowe, Characterization of tropospheric aerosols over the oceans with the NOAA advanced very high resolution radiometer optical thickness operational product, *J. Geophys. Res*., 102, 16889-16909, 1997.

Ignatov, A, *Personal Communication*, NOAA NESDIS ORA, Washington D.C., 20233, 1996.

Kasten, F., and A.T. Young, Revised optical air mass tables and approximation formula, *Appl. Optics*, 28, 4735-4738, 1989.

Kaufman, Y.J., Aerosol optical thickness and atmospheric path radiance, *J. Geophys. Res.*, 98, 2677-2692, 1993.

Kaufman, Y.J., A. Gitelson, A. Karnieli, E. Ganor, R.S. Fraser, T. Nakajima, S. Mattoo, and B.N. Holben, Size distribution and scattering phase function of aerosol particles retrieved from sky brightness measurements, *J. Geophys. Res.*, 99, 10341-10356, 1994.

King, M.D., D. Byrne, B. Herman, and J. Reagan, Aerosol size distributions obtained by inversion of spectral optical depth measurements, *J. Atmos. Sci.*, 35, 2153-2167, 1978.

King, M., D. Byrne, J. Reagan, and B. Herman, Spectral variation of optical depth at Tucson Arizona between August 1975 and December 1977, *J. Appl. Meteorol.*, 19, 16,639-16,650, 1980.

Klenk, K., P. Bhartia, E. Hilsenrath, and A. Fleig, Standard ozone profiles from balloon and satellite data sets, *J. Clim. Appl. Meteorol.*, 22, 2012-2022, 1983.

Li, X., H. Maring, D. Savoie, K. Voss, and J. Prospero, Dominance of Mineral Dust in Aerosol Light-Scattering in the North Atlantic Trade Winds, *Nature*, 380, 416-419, 1996.

Prospero, J.M., Saharan dust transport over the north Atlantic Ocean and Mediterranean, Chapter in*The Impact of Desert Dust From Northern Africa Across the Mediterranean*, Kluwer Academic Publishers, Oristano, Sardinia, 1995.

Reddy, P.J., F.W., Kreiner, J.J. DeLuisi, and Y. Kim, Aerosol Optical Depths Over the Atlantic Derived From Shipboard Sunphotometer Observations During the 1988 Global Change Expedition, *Global Biogeochem. Cycles*, 4, 225-240, 1990.

Savoie, D., and J. Prospero, Particle Size Distributions of Nitrate and Sulfate in the Marine Atmosphere, *Geophys. Res. Lett.*, 9, 1207-1210, 1982.

Savoie, D., Nitrate and non-sea-salt sulfate aerosols over major regions of the world oceans: concentrations, sources, and fluxes, *Ph.D. Dissertation*, Rosenstiel School of Marine and Atmospheric Science, University of Miami, 4600 Rickenbacker Causeway, Miami, Fl, 33149, 1984.

Savoie, D., J.M. Prospero, and E.S. Saltzman, Non-sea-salt sulfate and nitrate in trade wind aerosols at Barbados: evidence for long-range transport, *J. Geophys. Res.*, 94, 5069-5080, 1989.

Schlemmer, J., *Personal Communication*, Atmospheric Sciences Research Center, SUNY Albany, NY, 12205, 1996.

Shaw, G.E., Aerosols at Mauna Loa: Optical properties, *J. Atmos. Sci.*, 36, 862-869, 1979.

Smirnov, A., A. Royer, N. O'Neill, and A. Tarussov, A study of the link between synoptic air mass type and atmospheric optical parameters, *J. Geophys. Res.*, 99, 20967-20982, 1994.

Smirnov, A., Y. Villevalde, N. O'Neill, A. Royer, and A. Tarussov, Aerosol optical depth over the oceans: Analysis in terms of synoptic air mass types, *J. Geophys. Res.*, 100, 16639-16650, 1995.

Van de Hulst, H. C., *Light Scattering by Small Particles*, Dover Publications Inc., New York, NY, 1981.

Villevalde, Y.V., A.V. Smirnov, N.T. O'Neill, S.P. Smyshlyaev, and V.V. Yakovlev, Measurement of aerosol optical depth in the Pacific Ocean and the North Atlantic, *J. Geophys. Res.*, 99, 20983-20988, 1994.

Table 1

Location	Time Period
Miami, Florida Lat: 25.75 N Lon: 80.2 W Altitude: Sea Level	August 1993 to December 1995
Bermuda Lat: 32.38 N Lon: 64.7 W Altitude: Sea Level	August 1993 to December 1995
Barbados Lat: 13.18 N Lon: 59.43 W Altitude: Sea Level	August 1993 to December 1995

Table 2

Channel Number	Sunphotometer Filter Wavelength (nm)	Shadowband Filter Wavelength (nm)
1	380.2	Unfiltered (Broadband)
2	412.2	410
3	440.5	500
4	501.8	610
5	551.2	665
6	675.2	860
7	777.9	940
8	861.8	-
9	1025.9	-

Table 3

Location	nss Sulfate ($\mu g/m^3$)	Nitrate ($\mu g/m^3$)	Sea Salt ($\mu g/m^3$)	Dust ($\mu g/m^3$)
Miami	2.202	2.090	8.892	5.633
Bermuda	1.783	0.979	11.412	2.056
Barbados	0.765	0.599	19.997	14.864

Table 4a Monthly Miami AOD Results

Month-Year	$\bar{\tau}_{A_{500}}$	σ_τ	$\bar{\beta}$	σ_β	$\bar{\alpha}$	σ_α
Aug-93	-	-	-	-	-	-
Sep-93	0.114	0.024	0.070	0.022	0.734	0.228
Oct-93	0.142	0.068	0.069	0.020	0.976	0.374
Nov-93	0.142	0.020	0.080	0.011	0.833	0.001
Dec-93	0.121	0.034	0.050	0.013	1.269	0.056
Jan-94	0.121	0.030	0.071	0.005	0.740	0.398
Feb-94	0.120	0.035	0.083	0.035	0.566	0.375
Mar-94	0.151	0.073	0.069	0.030	1.063	0.240
Apr-94	0.166	0.038	0.104	0.035	0.706	0.553
May-94	0.243	0.091	0.111	0.033	1.098	0.319
Jun-94	0.163	0.058	0.128	0.057	0.217	0.457
Jul-94	0.234	0.055	0.209	0.034	0.148	0.100
Aug-94	0.075	0.013	0.059	0.011	0.347	0.319
Sep-94	0.127	0.058	0.079	0.026	0.524	0.773
Oct-94	0.119	0.054	0.056	0.027	0.987	0.509
Nov-94	0.093	0.039	0.049	0.014	0.762	0.713
Dec-94	0.097	0.041	0.093	0.019	-0.246	0.820
Jan-95	0.091	0.032	0.059	0.017	0.443	0.579
Feb-95	0.115	0.049	0.062	0.024	0.846	0.501
Mar-95	0.118	0.020	0.065	0.010	0.768	0.284
Apr-95	0.143	0.037	0.094	0.019	0.480	0.311
May-95	0.288	0.078	0.108	0.023	1.294	0.199
Jun-95	-	-	-	-	-	-
Jul-95	0.165	0.053	0.103	0.030	0.494	0.565
Aug-95	0.148	0.077	0.100	0.043	0.347	0.557
Sep-95	-	-	-	-	-	-
Oct-95	-	-	-	-	-	-
Nov-95	-	-	-	-	-	-
Dec-95	0.099	0.032	0.045	0.016	1.110	0.565
Total	0.141	0.050	0.084	0.034	0.684	0.367

Table 4b Monthly Bermuda AOD Results

Month-Year	$\bar{\tau}_{A_{500}}$	σ_τ	$\bar{\beta}$	σ_β	$\bar{\alpha}$	σ_α
Aug-93	-	-	-	-	-	-
Sep-93	0.161	0.043	0.104	0.015	0.603	0.290
Oct-93	0.161	0.041	0.103	0.020	0.622	0.232
Nov-93	0.117	0.025	0.081	0.018	0.540	0.214
Dec-93	0.160	0.037	0.102	0.009	0.614	0.304
Jan-94	0.099	0.012	0.069	0.011	0.531	0.298
Feb-94	0.102	0.023	0.079	0.005	0.322	0.372
Mar-94	0.157	0.041	0.099	0.026	0.666	0.268
Apr-94	0.169	0.050	0.105	0.022	0.667	0.415
May-94	0.134	0.047	0.085	0.030	0.655	0.259
Jun-94	0.270	0.125	0.170	0.072	0.599	0.233
Jul-94	0.116	0.072	0.081	0.045	0.474	0.179
Aug-94	0.126	0.131	0.097	0.125	0.424	0.334
Sep-94	0.100	0.061	0.049	0.035	1.058	0.746
Oct-94	0.075	0.041	0.060	0.015	0.288	0.663
Nov-94	0.068	0.021	0.077	0.016	-0.209	0.351
Dec-94	0.064	0.028	0.085	0.033	-0.920	0.973
Jan-95	0.081	0.035	0.075	0.023	-0.236	0.817
Feb-95	0.104	0.027	0.059	0.025	0.697	0.616
Mar-95	0.091	0.050	0.068	0.023	0.108	0.416
Apr-95	0.172	0.077	0.095	0.034	0.818	0.187
May-95	0.168	0.057	0.088	0.030	0.851	0.318
Jun-95	0.134	0.069	0.072	0.024	0.558	0.659
Jul-95	-	-	-	-	-	-
Aug-95	-	-	-	-	-	-
Sep-95	-	-	-	-	-	-
Oct-95	-	-	-	-	-	-
Nov-95	-	-	-	-	-	-
Dec-95	-	-	-	-	-	-
Total	0.129	0.047	0.086	0.025	0.442	0.433

Table 4c Monthly Barbados AOD Results

Month-Year	$\bar{\tau}_{A_{500}}$	σ_τ	$\bar{\beta}$	σ_β	$\bar{\alpha}$	σ_α
Aug-93	-	-	-	-	-	-
Sep-93	-	-	-	-	-	-
Oct-93	0.078	0.033	0.059	0.029	0.442	0.166
Nov-93	0.072	0.019	0.055	0.021	0.483	0.256
Dec-93	0.064	0.006	0.051	0.015	0.360	0.322
Jan-94	0.084	0.029	0.071	0.022	0.262	0.180
Feb-94	0.129	0.057	0.097	0.055	0.508	0.446
Mar-94	0.078	0.058	0.064	0.056	0.605	0.674
Apr-94	0.184	0.157	0.167	0.156	0.275	0.245
May-94	0.201	0.151	0.167	0.102	0.256	0.245
Jun-94	0.247	0.095	0.224	0.084	0.148	0.139
Jul-94	0.362	0.128	0.267	0.111	0.504	0.225
Aug-94	0.210	0.067	0.132	0.055	0.731	0.211
Sep-94	0.169	0.090	0.118	0.076	0.640	0.287
Oct-94	-	-	-	-	-	-
Nov-94	-	-	-	-	-	-
Dec-94	-	-	-	-	-	-
Jan-95	-	-	-	-	-	-
Feb-95	-	-	-	-	-	-
Mar-95	-	-	-	-	-	-
Apr-95	-	-	-	-	-	-
May-95	-	-	-	-	-	-
Jun-95	0.257	0.107	0.260	0.108	0.014	0.059
Jul-95	0.144	0.060	0.147	0.063	0.047	0.187
Aug-95	0.200	-	0.176	-	0.138	-
Sep-95	-	-	-	-	-	-
Oct-95	-	-	-	-	-	-
Nov-95	-	-	-	-	-	-
Dec-95	-	-	-	-	-	-
Total	0.165	0.085	0.137	0.073	0.361	0.220

Table 5

Location - Dominate Aerosol	α	σ_α
Miami - nss Sulfate	1.216	0.209
Bermuda - nss Sulfate	1.012	0.292
Miami - Sea Salt	0.205	0.202
Bermuda - Sea Salt	0.580	0.376
Barbados - Sea Salt	0.406	0.080
Miami - Dust	0.280	0.235
Bermuda - Dust	0.585	0.127
Barbados - Dust	0.339	0.268

Table 6

AOD (500 nm)	Angstrom Exponent	Primary Aerosol Species
0.0 - 0.2	0.0 - 0.5	sea-salt or dust
	> 0.5	indeterminate
> 0.2	0.0 - 0.5	dust
	0.5 - 1.0	indeterminate
	> 1.0	non-sea-salt sulfate

Figure 1a

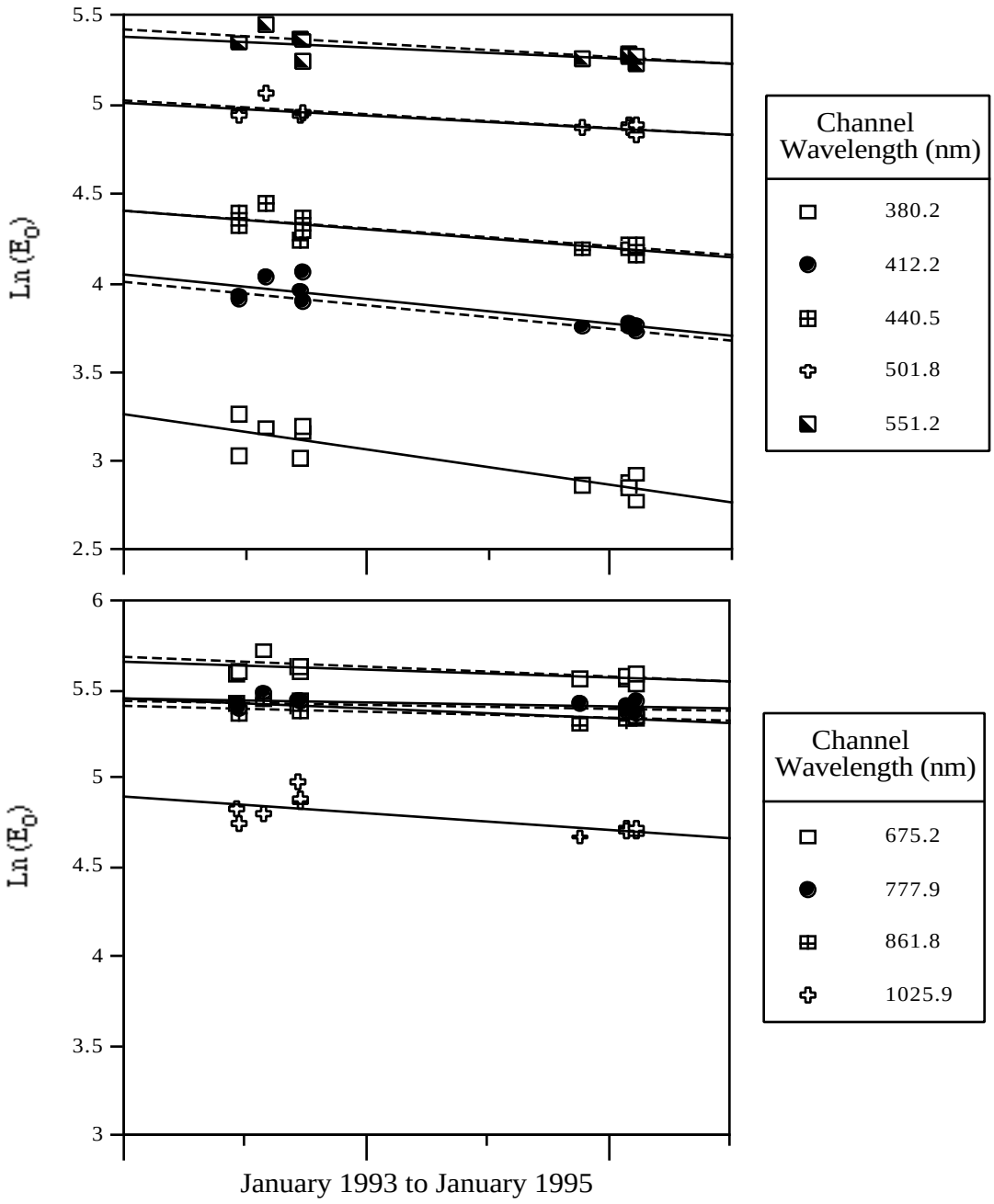

Figure 1a. Calibration history for the Miami sunphotometer. The solid line is the fit to the Langley and cross-calibrations. The dotted line is the fit to the error corrected calibrations.

Figure 1b

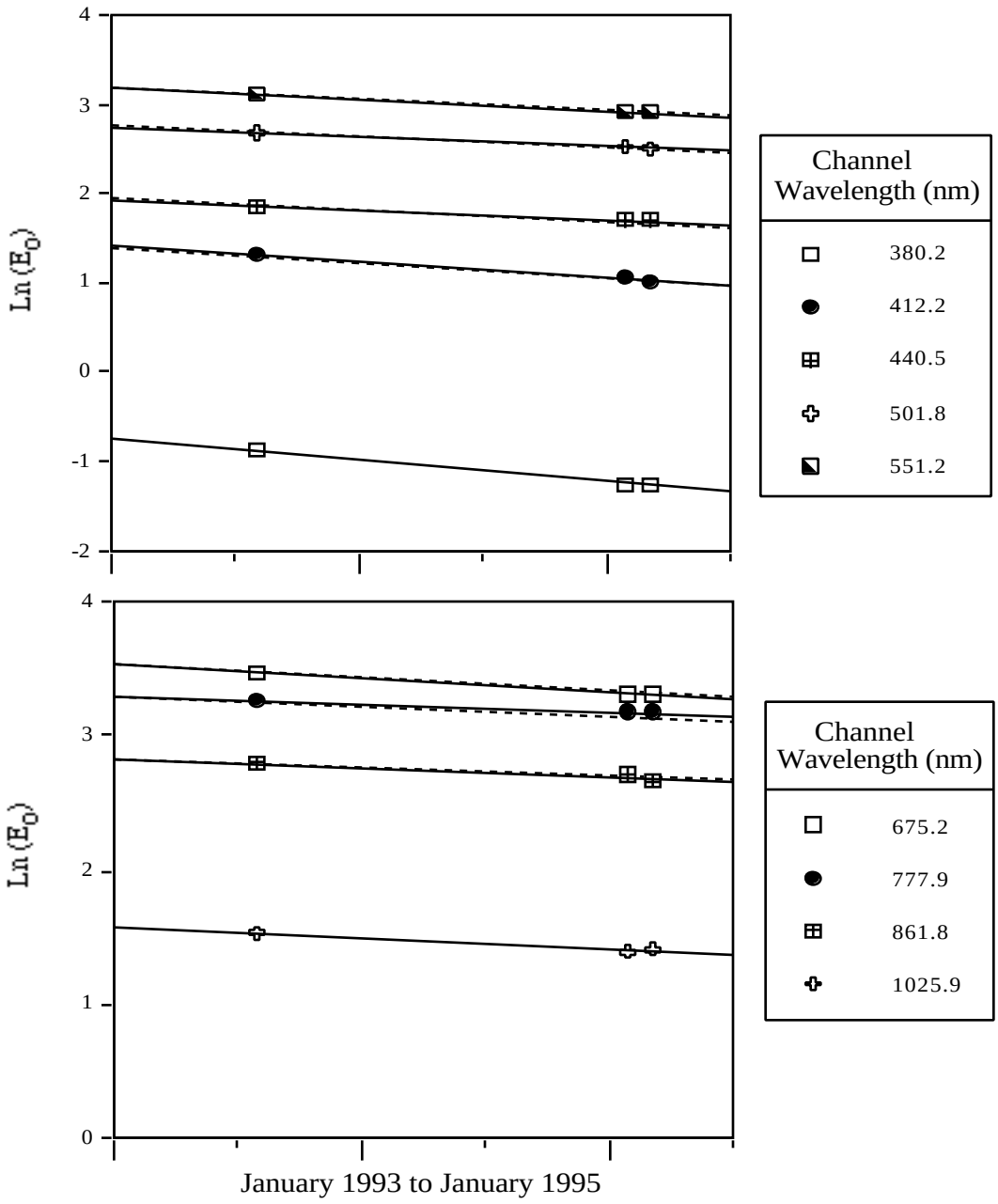

Figure 1b. Calibration history for the Bermuda sunphotometer. The solid line is the fit to the Langley and cross-calibrations. The dotted line is the fit to the error corrected calibrations.

Figure 1c

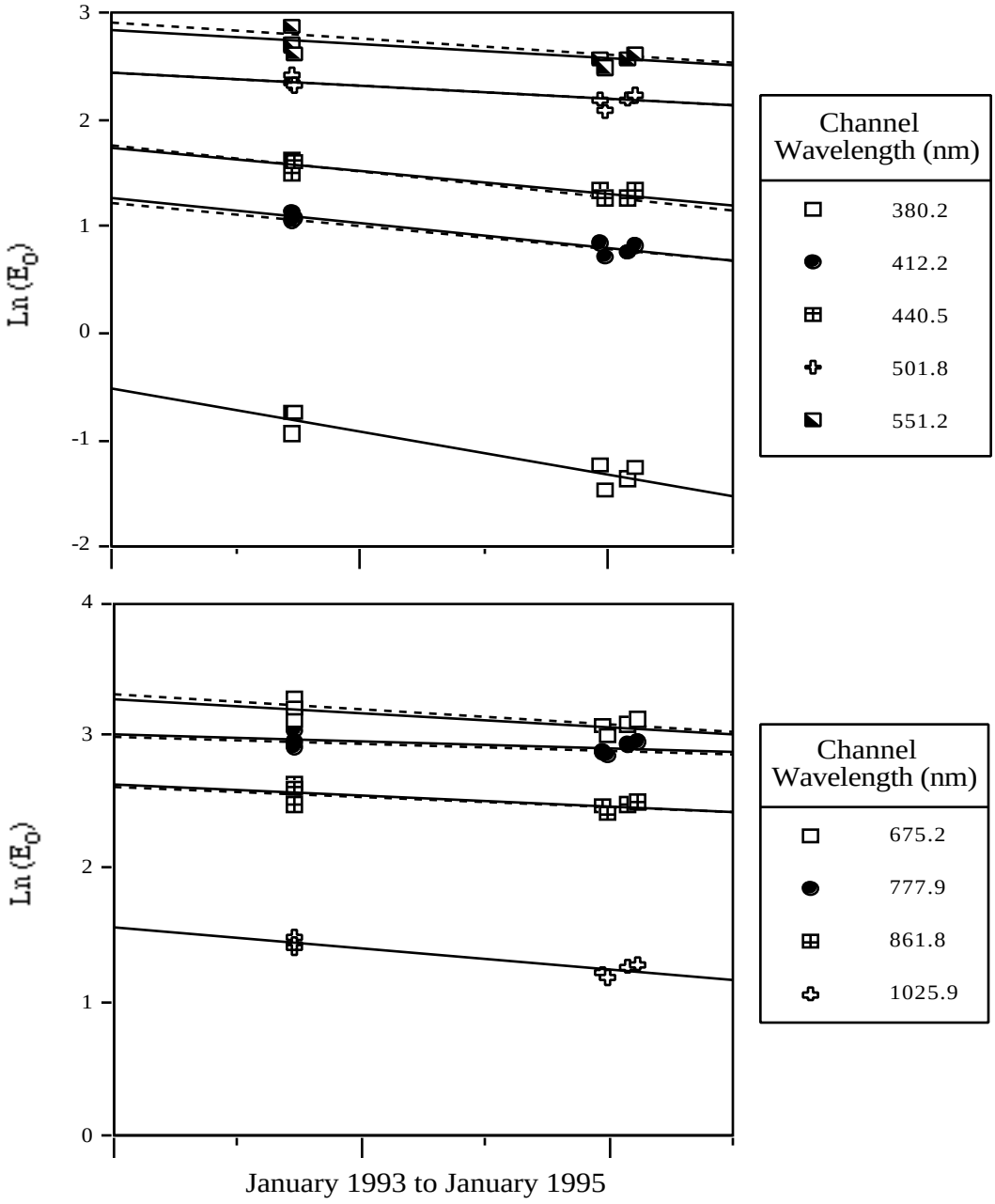

Figure 1c. Calibration history for the Barbados sunphotometer. The solid line is the fit to the Langley and cross-calibrations. The dotted line is the fit to the error corrected calibrations.

Figure 2a

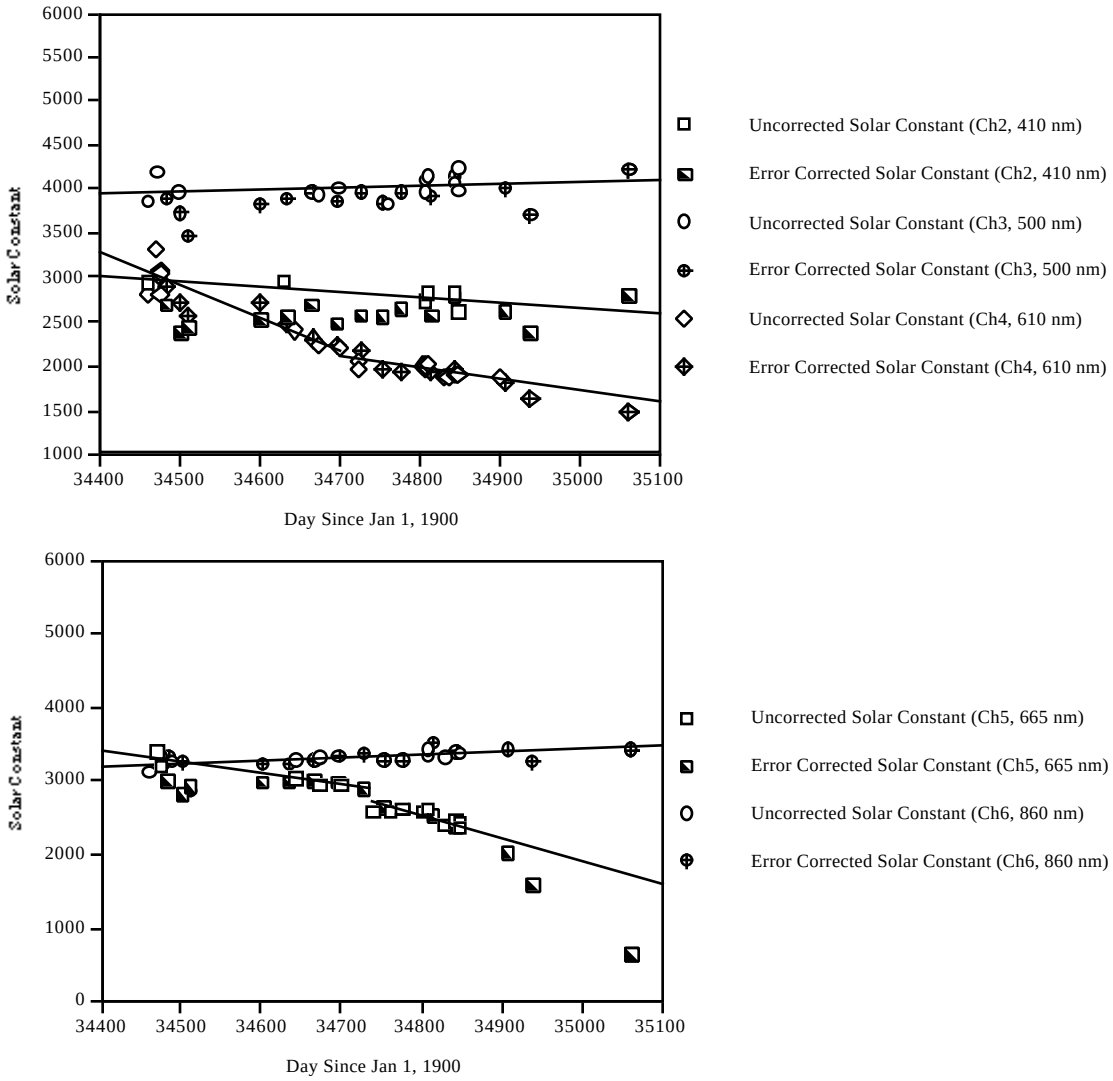

Figure 2a. Calibration history for the Miami shadowband (May 1994 to December 1995). The solid line is the fit to the OLRA Langley calibrations.

Figure 2b

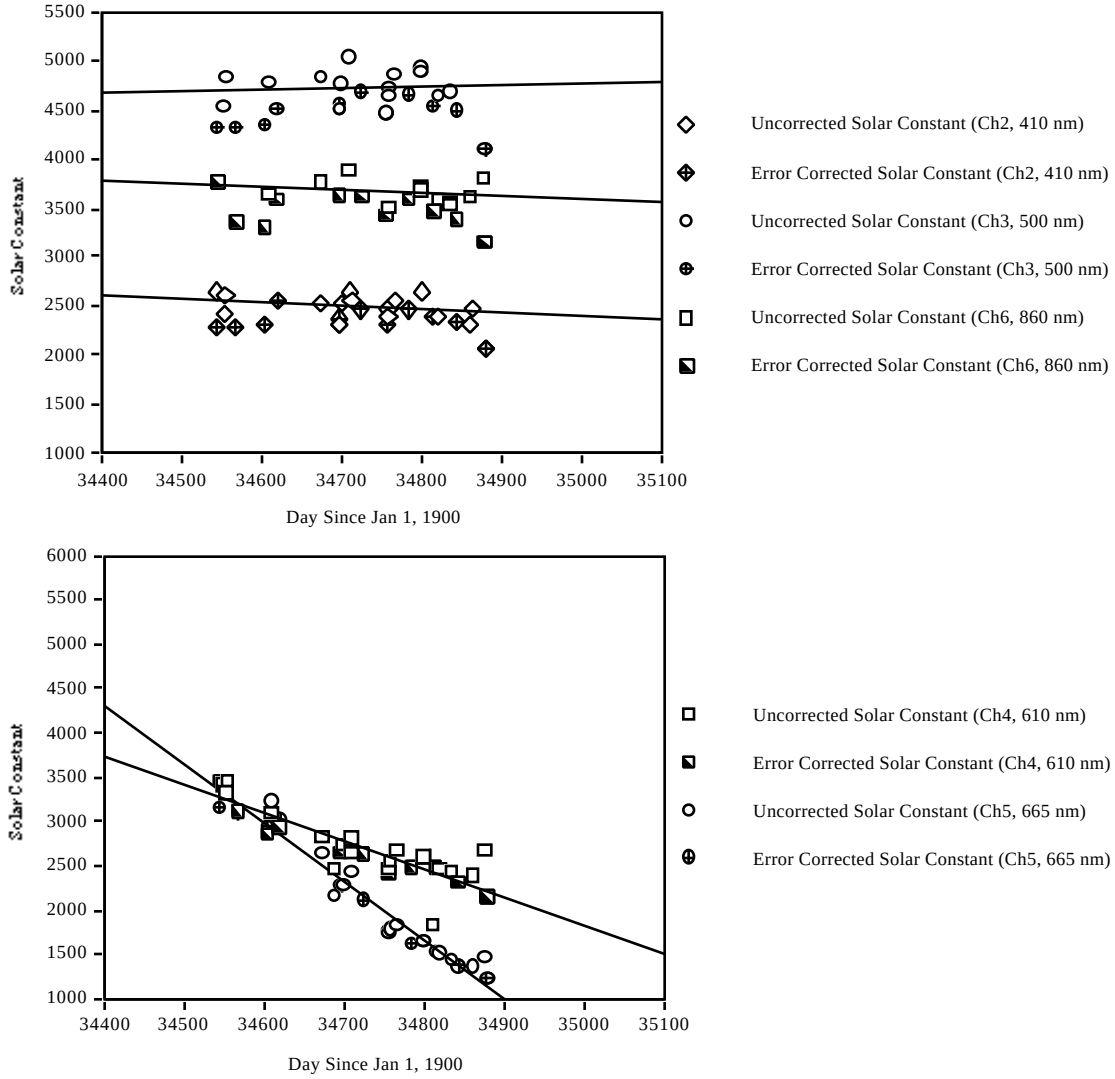

Figure 2b. Calibration history for the Bermuda shadowband (May 1994 to December 1995). The solid line is the fit to the OLRA Langley calibrations.

Figure 2c

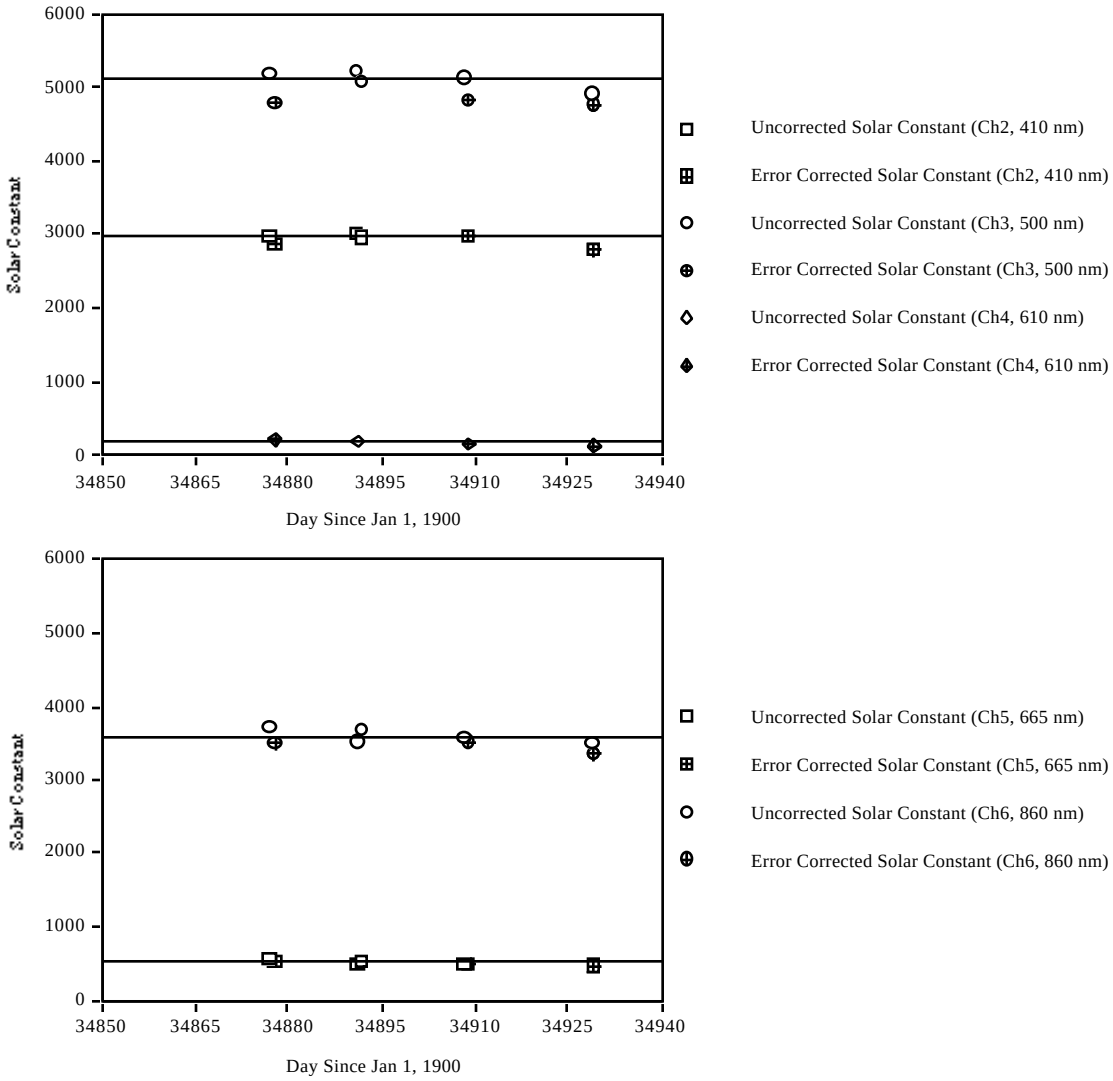

Figure 2c. Calibration history for the Barbados shadowband (June 1995 to August 1995). The solid line is the fit to the OLRA Langley calibrations.

Figure 3a

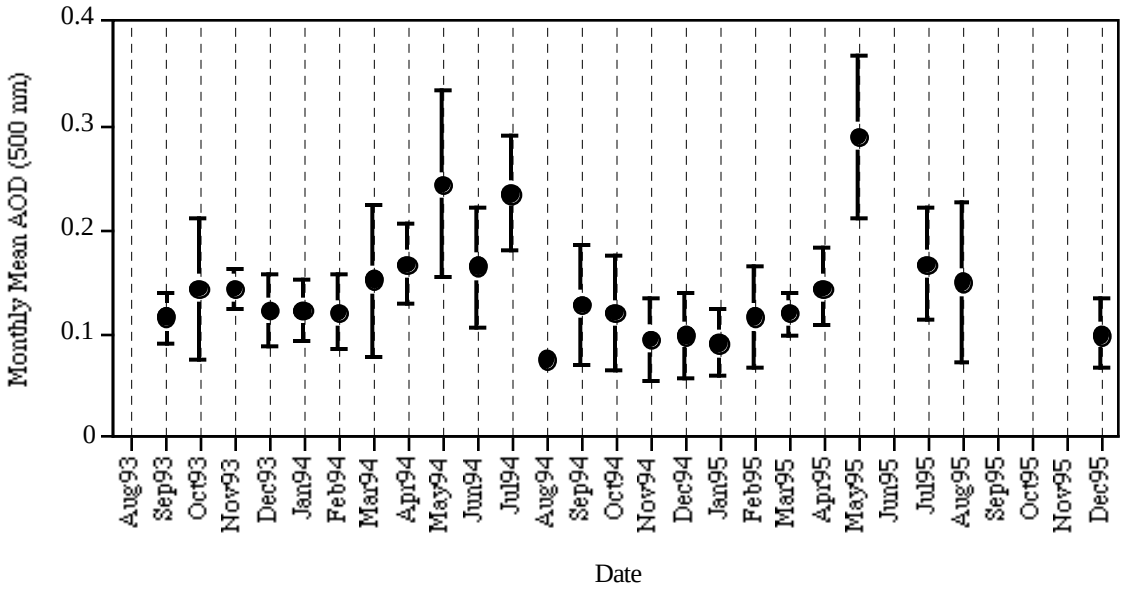

Figure 3a. Miami monthly mean AOD (500 nm) and corresponding standard deviations from August 1993 to December 1995.

Figure 3b

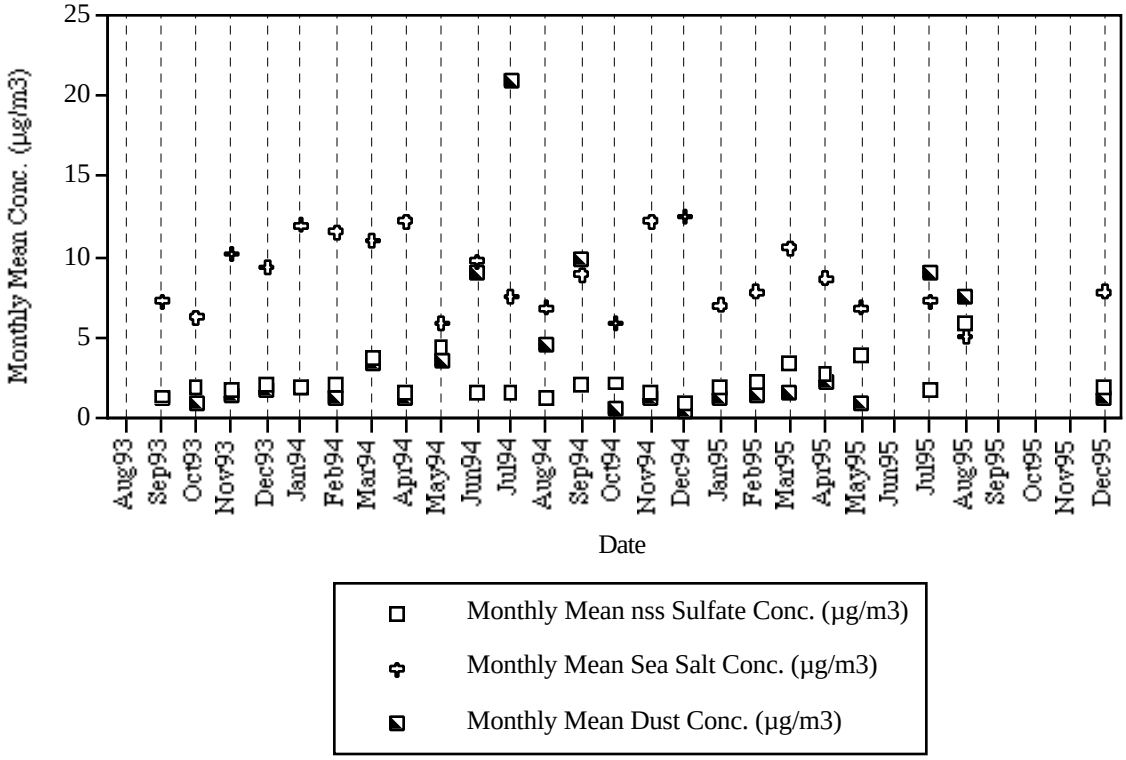

Figure 3b. Miami monthly mean aerosol concentrations from August 1993 to December 1995.

Figure 4a

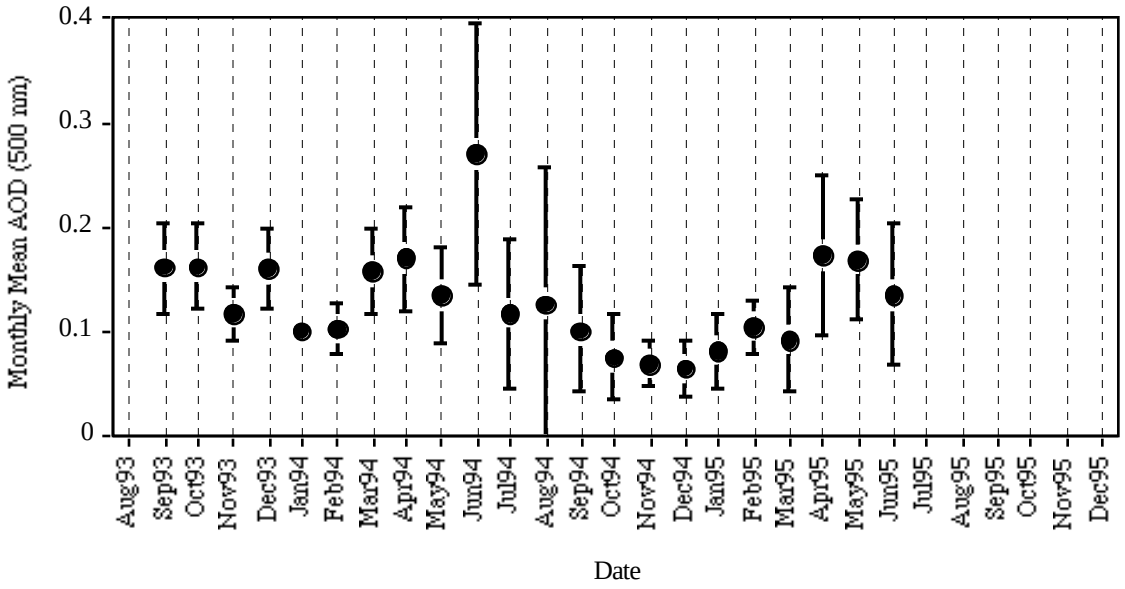

Figure 4a. Bermuda monthly mean AOD (500 nm) and corresponding standard deviations from August 1993 to December 1995.

Figure 4b

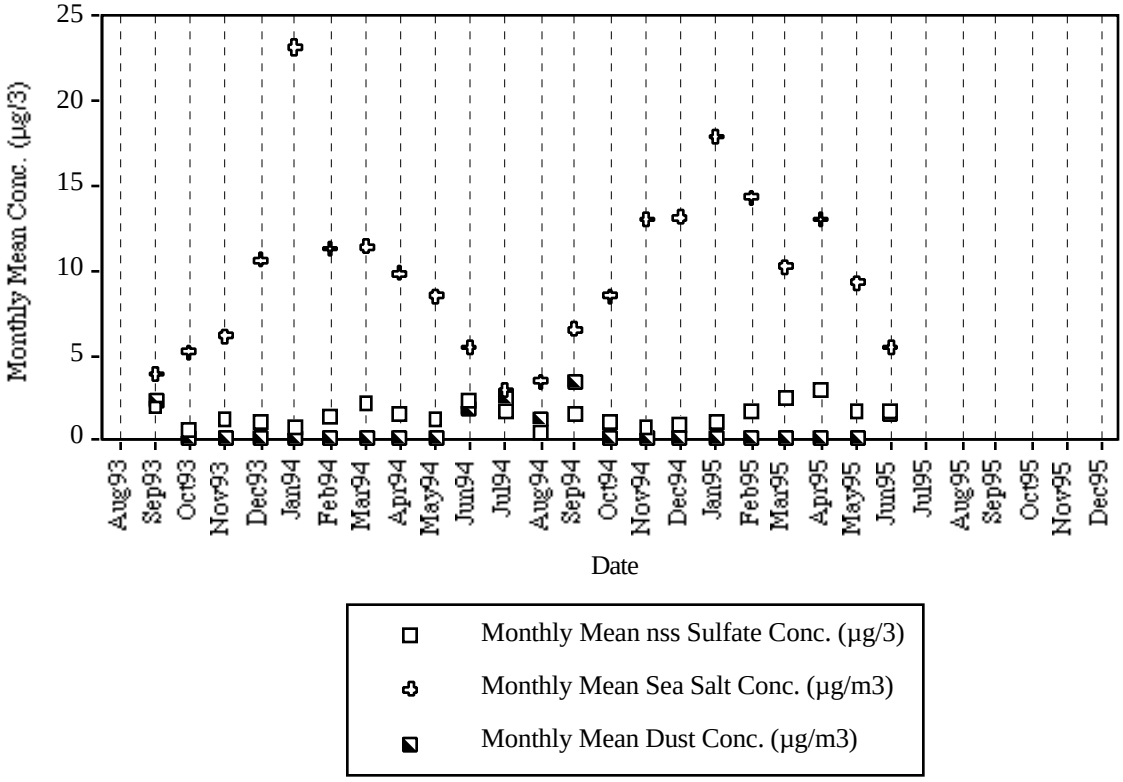

Figure 4b. Bermuda monthly mean aerosol concentrations from August 1993 to December 1995.

Figure 5a

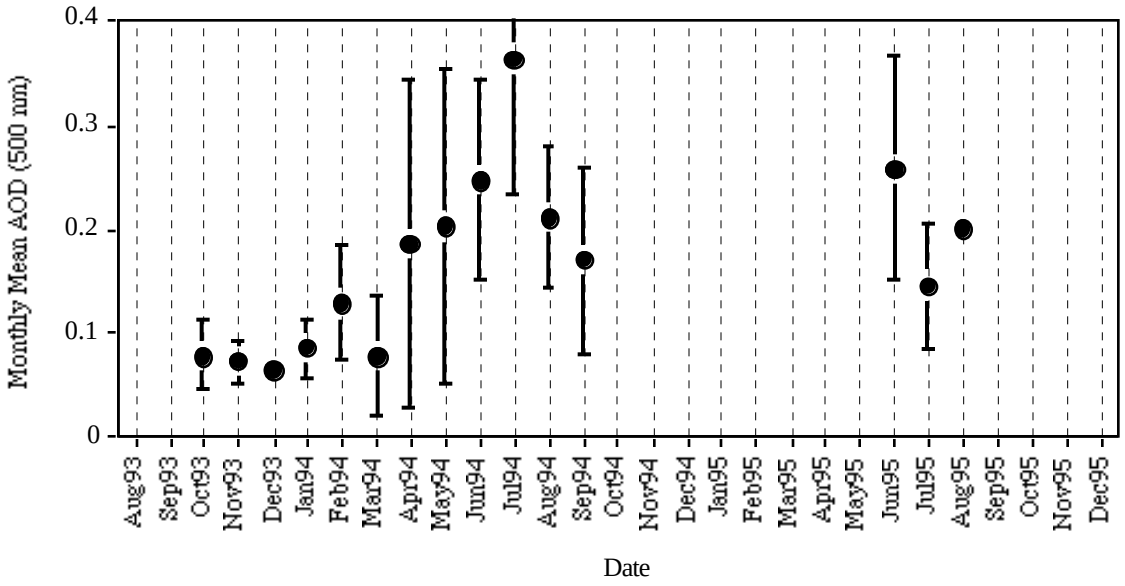

Figure 5a. Barbados monthly mean AOD (500 nm) and corresponding standard deviations from August 1993 to December 1995.

Figure 5b

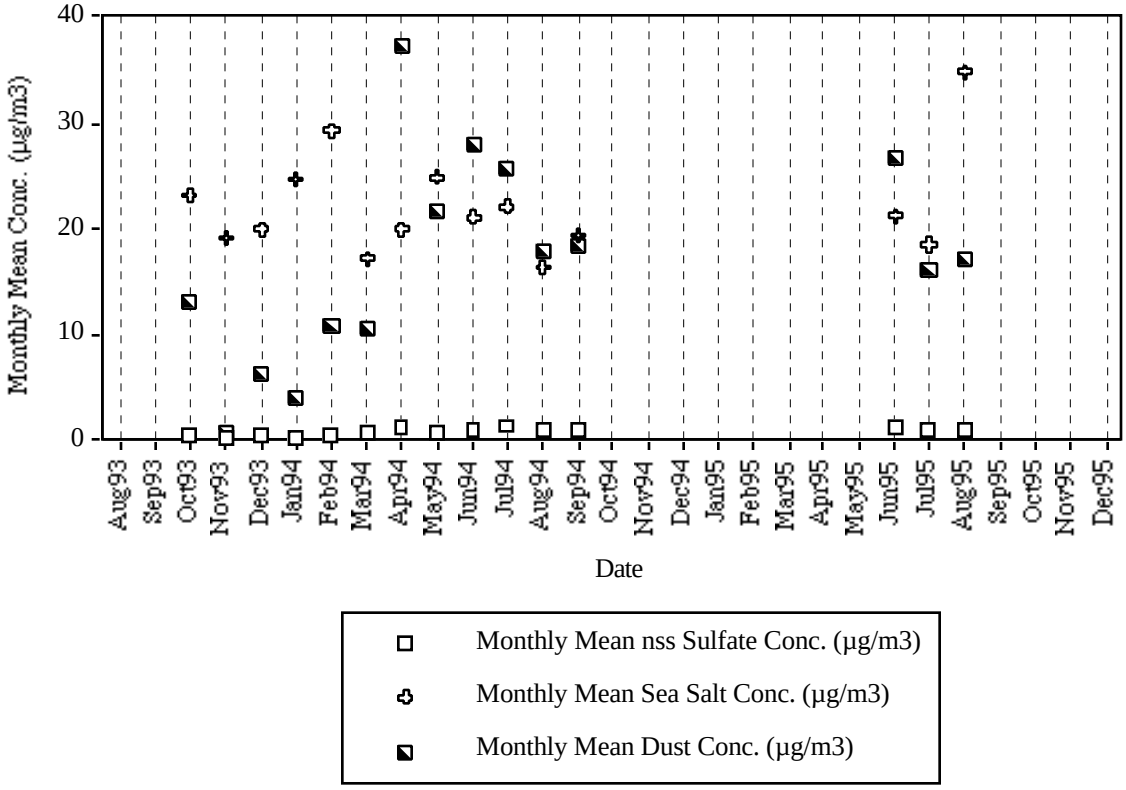

Figure 5b. Barbados monthly mean aerosol concentrations from August 1993 to December 1995.

Figure 6a

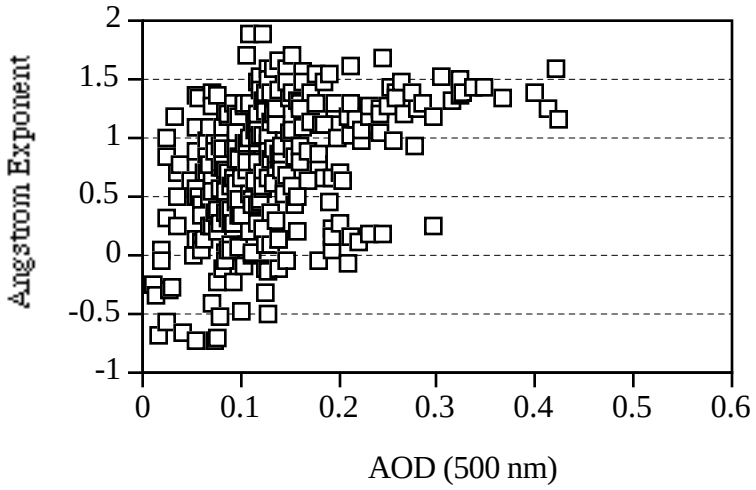

Figure 6a. Miami daily averaged AOD (500 nm) versus the Angstrom exponent.

Figure 6b

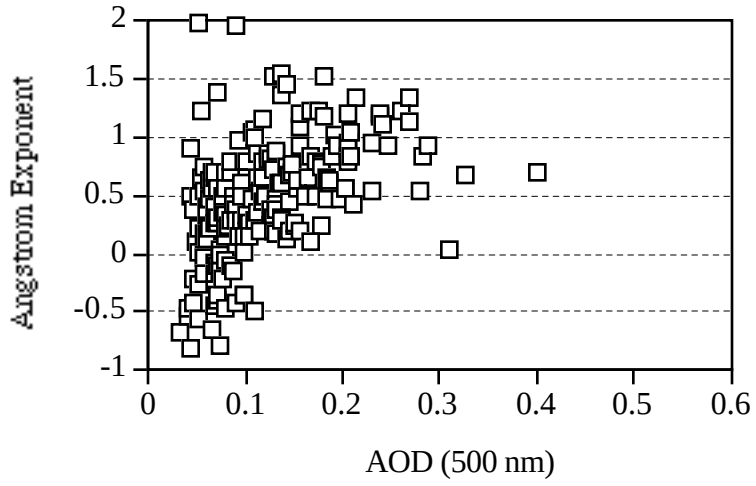

Figure 6b. Bermuda daily averaged AOD (500 nm) versus the Angstrom exponent.

Figure 6c

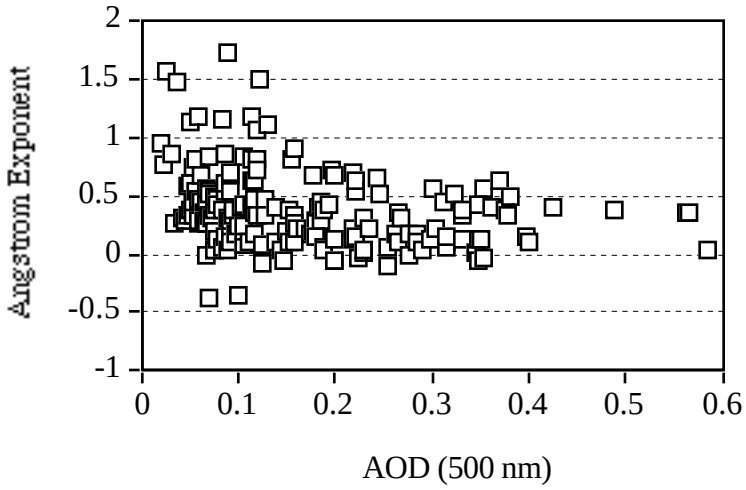

Figure 6c. Barbados daily averaged AOD (500 nm) versus the Angstrom exponent.

Figure 7a

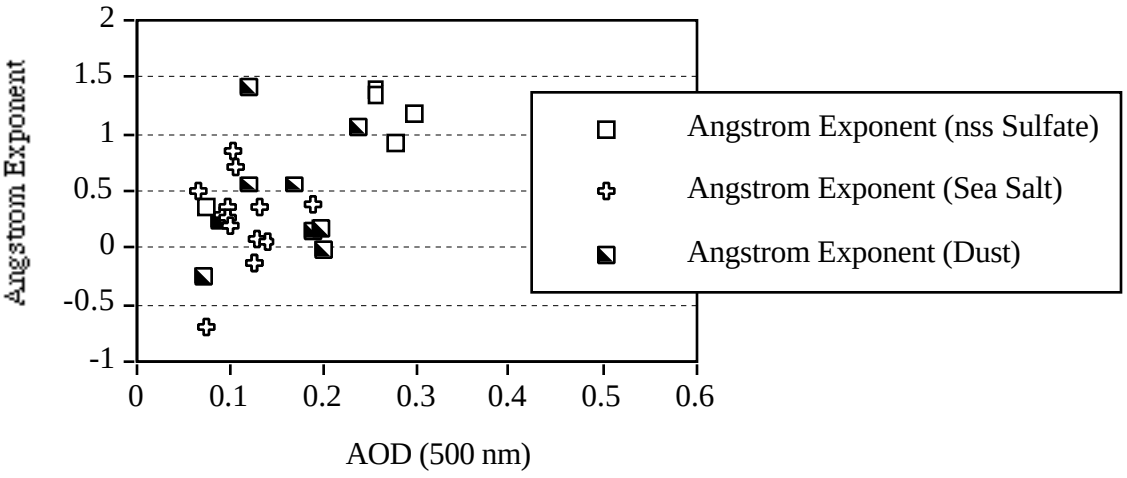

Figure 7a. Dominant aerosol correlation results: Miami daily averaged AOD (500 nm) versus the Angstrom exponent.

Figure 7b

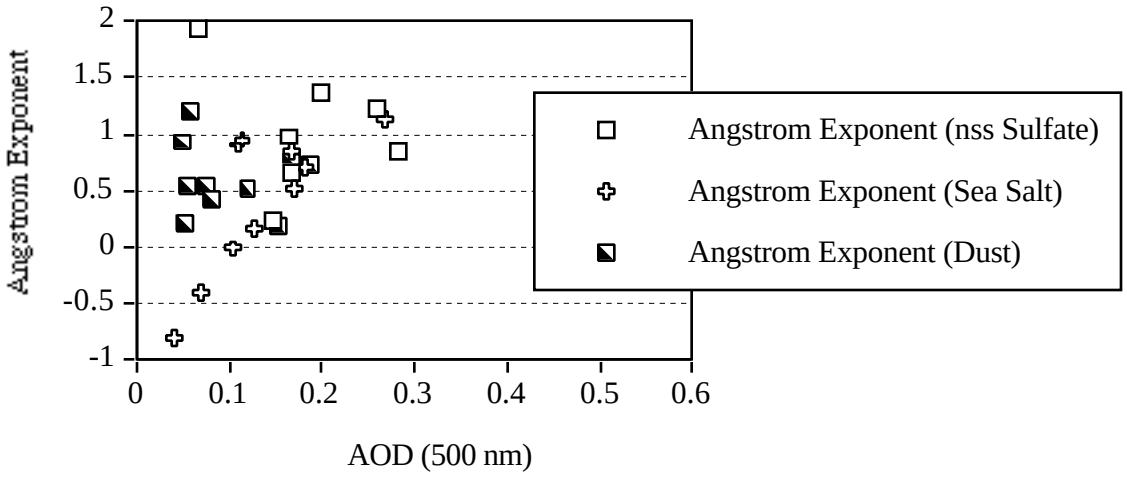

Figure 7b. Dominant aerosol correlation results: Bermuda daily averaged AOD (500 nm) versus the Angstrom exponent.

Figure 7c

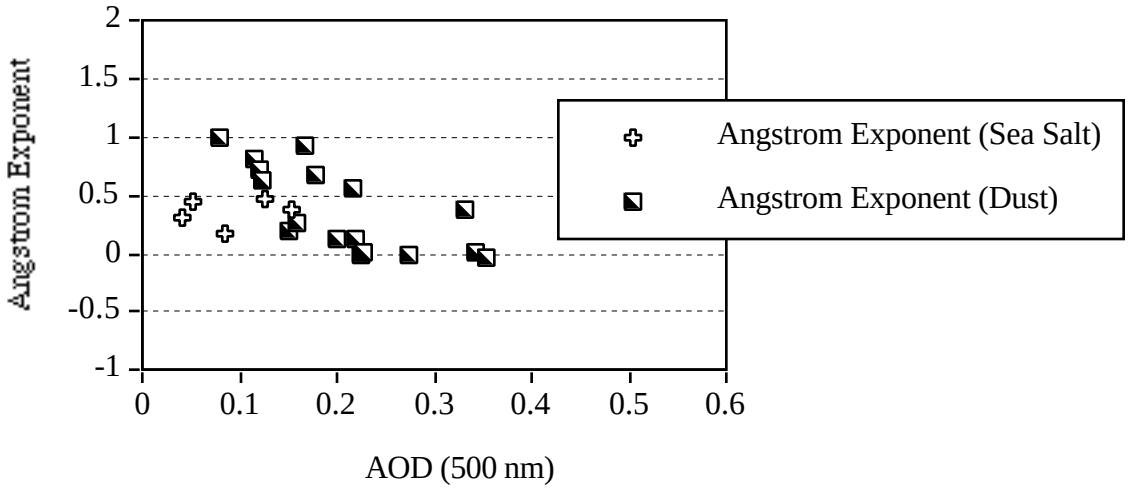

Figure 7c. Dominant aerosol correlation results: Barbados daily averaged AOD (500 nm) versus the Angstrom exponent.

Figure 8

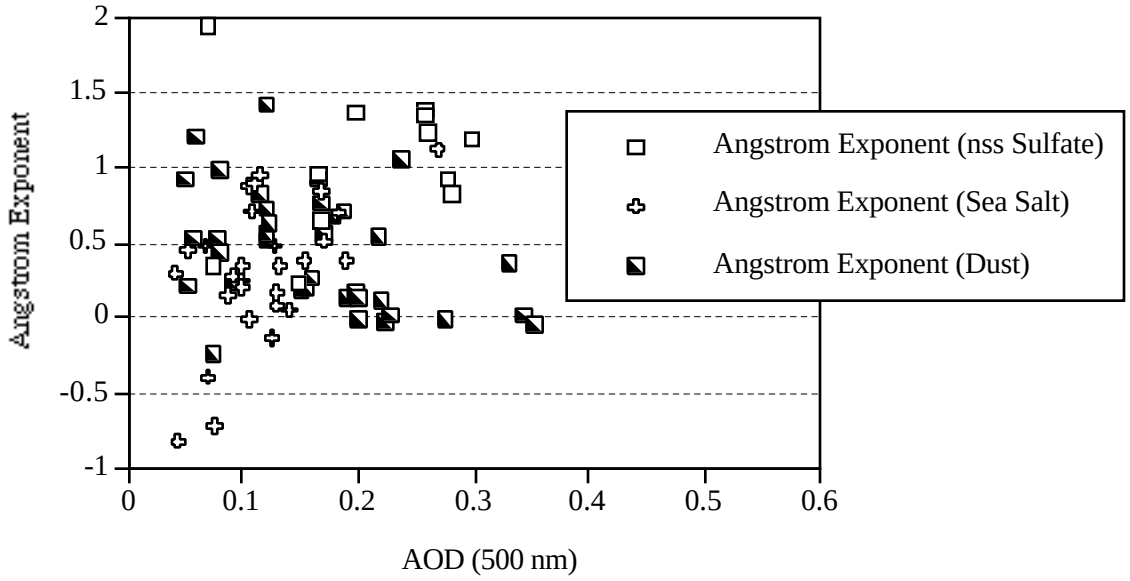

Figure 8. Dominant aerosol correlation results: Combined Miami, Bermuda, and Barbados daily averaged AOD (500 nm) versus the Angstrom exponent.